Optimal Movement and Timing in BMX Starts

A Predictive Optimal Control Study

BM51035: BME MSc Thesis

J.C. d'Aumerie

Delft University of Technology

Optimal Movement and Timing in BMX Starts

A Predictive Optimal Control Study

by

J.C. d'Aumerie

to obtain the degree of Master of Science
at the Delft University of Technology,
to be defended publicly on **Wednesday July 10, 2024 at 10:45 AM**

Student number:	5152399	
Submission date:	July 5, 2024	
Faculty:	Mechanical Engineering	
Thesis committee:	Dr. Ir. A. Seth	TU Delft
	Dr. Ir. Van Wouwe	TU Delft
	Dr. Ir. A.L. Schwab	TU Delft

An electronic version of this thesis is available at http://repository.tudelft.nl/

Image on front cover taken from velozine.nl:
https://www.velozine.nl/specials/bmx-supercross-papendal/

TU Delft

Preface

J.C. d'Aumerie
Delft, July 2024

This thesis marks the culmination of my research journey in the field of biomechanics and optimal control, focusing on the dynamic challenges faced by BMX riders during the start phase of a race. The journey towards this moment has been challenging, but I am grateful to have worked on a project so close to my interests in cycling. It has been a privilege to collaborate with the Dutch National BMX Team, the National Training Facility Papendal, and the Royal Dutch Cycling Union (KNWU). First and foremost, I would like to express my gratitude to my supervisors, Ajay Seth and Tom van Wouwe, whose guidance, support, and encouragement have been instrumental in the completion of this work. Their expertise and critical feedback have significantly shaped this research, pushing me to explore deeper and think more critically. Furthermore, I would like to thank Ina Janssen from Papendal and Kevin van der Linde from the KNWU for their invaluable advice and input during the project. I am also grateful to Jan Groenhuis for sharing his work and the BMX plus rider model with me. I extend my thanks to Adam Kewley for providing access to the CBL workstation, which significantly decreased the computational time of my optimizations, and for his prompt assistance whenever I encountered problems with OpenSim Creator. I would also like to thank all members of the Computational Biomechanics Lab for their valuable feedback and input during our weekly meetings. I am deeply thankful to my parents, Mieke and Rombout, and my siblings, Boudewijn and Monica, for their words of encouragement, unwavering support, and belief in a successful completion of my thesis without exerting too much pressure on me. Finally, I owe immense gratitude to Katinka, who has been the loveliest throughout this entire process. Thank you for your patience, encouragement, and all the delicious snacks and meals, especially as the end approached. I do not know how I would have done this without you.

Abstract

Introduction The BMX start is crucial in BMX racing, often determining race outcomes. This study focuses on optimizing BMX gate starts using predictive optimal control techniques, examining the effects of maximal crank torque and reaction time on performance.

Objective: To gain insights into the optimal kinematics and dynamics of BMX starts by analysing the impact of rider strength through varying maximal crank torque and reaction time using a simplified model. Additionally, to validate a complete BMX rider-plus-bicycle model and solve a predictive optimal control problem using the same objective function as for the simplified model.

Method: Two models were employed: the 'Upper Body Model' for analysing varying crank torques and reaction times, and the 'Full Body Model' for providing a better biomechanical representation of the rider and the produced crank torque. The 'Upper Body Model' simplifies the rider's lower body, replacing leg-generated forces with an ideal actuator at the cranks, reducing computational complexity. Optimal control problems were solved for maximal crank torques of 250 Nm, 275 Nm, 300 Nm, 325 Nm, and 350 Nm, and for reaction times of 0.14 s, 0.16 s, and 0.18 s with a 300 Nm crank torque. The objective was to maximize the bicycle's final position and linear velocity after 1.5 s, while minimizing control efforts and pitch angle. The 'Full Body Model' included the rider's legs to accurately reproduce crank torque. This model was validated with an optimal tracking simulation, minimizing the differences between experimental joint angles and simulation results. A predictive optimal control problem was solved with the same objective as for the 'Upper Body Model'.

Results: The gate's falling speed was a limiting factor during the start, with bicycle velocities matching the gate's speed until it was halfway open. Simulations with lower maximal crank torque showed an increased recoil (backward movement). With a smaller maximal crank torque, the propulsive force is less, requiring more distance to propel the bicycle to match the gate drop velocity. Therefore, the initial position in simulations with lower maximal crank torques, had the centre of mass positioned further backward to enhance the backward propulsion of the bicycle, leveraging the conservation of momentum.

Improved reaction time led to slightly better BMX start performance but did not necessitate a change in start technique, as the joint torques remained consistent (with a small phase shift corresponding to the reaction time).

The 'Full Body Model' closely tracked experimental kinematics with a mean RMSE of 2.28°, showing an RMSE of 61.14 Nm for crank torque during the tracking optimization and 59.41 Nm in the predictive simulation. The predictive simulation showed significant improvements in BMX start performance, with a time to kink (at 3.15 m) of 1.16 s compared to 1.23 s, with the lead being taken at the gate drop. The recoil employed was considerably greater compared to experimental data (13 cm vs 8 cm).

Conclusion: The developed framework for using predictive optimal control in BMX start research provides a systematic basis for future studies. Insights from this study can be applied to training strategies focusing on technique, timing, and initial position. Future research could explore the influence of leg strength, gear ratios, and crank lengths on BMX start performance.

Contents

List of Figures

List of Tables

1

Introduction

1.1. BMX Racing

Bicycle Moto-Cross (BMX) Supercross (SX) racing is a relatively new sport, that originated in the late 1960s. It is inspired by the motocross sport in California (United States) when children began riding their bicycles on self-made dirt tracks. Eventually, it evolved into a sport category, leading to the development of specialized tracks and bicycles, and the organization of BMX competitions [1]. BMX gained popularity in the 1980s, largely due to the newly created X Games, which were broadcast on television. In 1981, the International Federation of BMX was established, and the sport developed rapidly. The first world championships were held in 1982 in Dayton (United States), and BMX racing has been an Olympic event since the Beijing Olympics in 2008 [1]. Since becoming an Olympic sport, more scientific research has focused on BMX racing.

In BMX racing the goal is to complete a dirt track (350-400 m in length) as fast as possible. The start is very decisive for race outcome [2]. An elite BMX race typically takes between 30 and 50 s [3]. The track consists of a start ramp followed by a straight section, three sharp banked corners, jumps, and hills (Figure 1.1.1a). While tracks can vary, the BMX start ramp is standardized (Figure 1.1.1b) [4].

Figure 1.1.1: BMX SX Track (a) and Start Gate (b) at Sport Centre Papendal, Arnhem, The Netherlands. Photo adopted from papendal.nl, accessed in 2023.

BMX SX is the Olympic category of BMX racing, distinguished by an 8-meter-high start ramp with a minimum width of 10 meters. The first 3.15 meters have an incline of 18 degrees, followed by a sudden increase to 28 degrees. The point where the slope increases is called the ‘kink’ [4].

All races start with a standing mass-start from an electronically controlled starting gate, with a maximum of eight riders per heat. The starting procedure consists of the phrase, “Ok riders, Random start. Riders ready? Watch the gate.” After the word ’gate’, there is a random delay between 0.1 and 2.7 s, followed by four tones that coincide with the display of a light tree (red, yellow, yellow, green) (Figure 1.1.2). The gate begins to fall on the last tone and the green light [4].

The start can be divided into two main parts: the backward motion of the bicycle, known as the recoil phase, and the forward acceleration phase. The recoil phase is often referred to as the ’slingshot’

manoeuvre. During this manoeuvre, riders rapidly shift their bodies forward, causing the bicycle to move slightly backward. This backward motion creates the necessary space for gathering forward velocity before the gate drop [5].

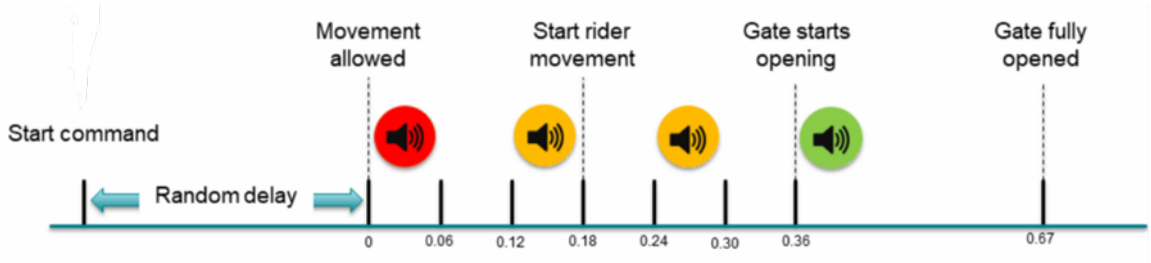

Figure 1.1.2: The BMX Gate Start Sequence According to the UCI Rules & Regulations. Adapted from Groenhuis [6]

Kalichová *et al.* [7] conducted a biomechanical analysis of the BMX gate start. They divided the start into five distinct phases, recording the duration of each phase for two BMX riders (one male and one female) (Figure 1.1.3). The duration of each phase was very similar for both riders. The five phases of the BMX start, as outlined by Kalichová *et al.* [7], are as follows:

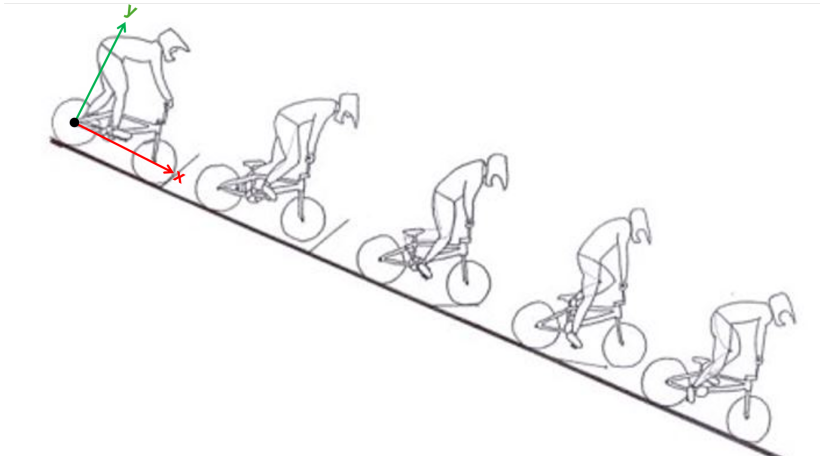

Figure 1.1.3: Five Phases of the BMX Start. This figure breaks down the BMX start into five distinct phases, highlighting key movements and positions. The phases are,1: Reaction time, 2: Preparation movement, 3: First pedal stroke, 4: Dead point pedal passage and 5: Second pedal stroke. The x-axis of the bicycle frame is oriented alongside the start ramp and the y-axis perpendicular to the start ramp. Adapted from Kalichová *et al.* [7].

Phase 1 - Reaction Time: This phase begins with the first red light and ends at the moment of movement initiation.

Phase 2 - Preparation Movements: Starting from the initiation movement and continues until the first pedal stroke. The movement of the first pedal stroke is delayed compared to the movements of the upper body. The rider's centre of mass shifts forward, causing the bicycle to experience a slight backward roll due to the conservation of momentum, commonly referred to as the recoil.

Phase 3 - First Pedal Stroke: This phase begins at the moment of the first pedal stroke and continuing until its completion, where the cranks are perpendicular to the ground. In this phase, the movement of the lower limbs dominates, with the first foot pushing the pedal down while the back foot pulls it up.

Phase 4 - Dead Point Pedal Passage: This phase is the time delay between the first and second pedal strokes. The cranks are oriented perpendicular to the ground in the top dead centre and bottom dead centre. In this position, it is difficult to exert a tangential force at the crank, resulting in a delay between the first and second pedal strokes. During this phase, the riders move their pelvis backward and extend their hips, simultaneously pushing the bicycle forward.

Phase 5 - Second Pedal Stroke: This phase starts at the onset of the second pedal stroke and

continues until its completion. The crank is rotated by an angle of 180 degrees, in contrast to a rotation of 90 degrees during the first pedal stroke. This phase is characterized by the dominant work of the lower limbs, with one foot exerting a pushing force and the other foot exerting a pulling force, leading to accelerated crank movement.

1.1.1. The Importance of the BMX Start

The start is the most crucial phase in BMX racing [2] because, being ahead of opponents at the bottom of the ramp, reduces the likelihood of crashing due to contact with other riders and enables the rider to take the optimal line through the corners [8], [9].

Rylands and Roberts [2] analysed the positions of 348 riders across 175 UCI World Cup Races at four intermediate checkpoints. They found a moderate strong significant positive correlation (Kendall's tau-b bivariate correlation, $\tau = 0.271, p < 0.01$) between the top three riders at the first checkpoint (1.0746 $\pm$ 0.8159 s into the race) and the top three riders at the end of the race. This first checkpoint is approximately at the position of the kink.

Additionally, they identified a stronger, significant positive correlation between the top three riders at the second checkpoint (8-10 s into the race) and the top three riders at the end of the race (Kendall's tau-b bivariate correlation, $\tau = 0.586, p < 0.01$). This second checkpoint is roughly halfway through the first corner.

To gain a competitive advantage at the start ramp, BMX SX riders demonstrate impressive performance metrics. In the study by Herman *et al.* [10], Olympic BMX riders delivered a mean peak power of, 2087 $\pm$ 157 Watts with a high peak cadence of 212 $\pm$ 4 rev/min at the start ramp. Race analysis indicates that elite BMX riders reach high velocities at the bottom of the start ramp. On average, male riders attain velocities of approximately 56.89 km/h within 2.62 s, while female cyclists reach speeds of about 52.90 km/h within 2.74 s [11].

Due to the high correlation between start performance and finishing position, the majority of training time is spent on improving the gate start, by training the physical strength and technique of the riders [11], [12]. The 'kink time' is often measured to quantify gate start performance, defined as the time taken to reach the kink at approximately 3 meters from the start [12]. Strength training focuses on exercises that strengthen the hip and knee extensors, the muscle groups mostly used during the start and pedalling [11].

An experimental study by Gross *et al.* [5] found that an early slingshot manoeuvre (recoil) during the preparation movement before the gate drop and a powerful first pedal stroke, with both high torque and high cadence, had the most influence on overall starting performance. The time until the initiation of forward velocity (t_{v_0}) and the distance of the bicycle behind the start line after the gate drop ($d|_{t_0}$) were measured to evaluate the effectiveness of the slingshot. Both t_{v_0} and $d|_{t_0}$ were significantly correlated with the bicycle's velocity at the gate drop.

Figure 1.1.4: Trajectory of the Front Wheel Hub During BMX Start. The figure displays the path of the front wheel hub during the start. BMX rider moves from left to right. Adapted from Grigg [13].

Grigg [13] found that a greater recoil distance correlated with a faster time to the kink. She determined the kinematics using Kinovea, a video analysis software, from video footage of the start. The trajectories of the front hub were plotted, revealing that the fastest riders employed a start technique that resulted in a hairpin-shaped trajectory of the front hub (Figure 1.1.4. Other front hub trajectories identified were 'up and over' and 'half cycle' (Figure 1.1.4). The position at the start where the BMX rider had a large shoulder angle, straight arms and bent knees was most likely to result in a start with a hairpin-shaped front hub trajectory.

Janssen *et al.* [14] reported strong, significant positive correlations between the vertical velocity of the bicycle at the gate drop and the start performance, defined as the distance covered after one second. Additionally, greater mass and frontal area were significantly positively correlated with velocity at the start [5]. This correlation could be attributed to the fact that larger riders, who have greater muscle mass, are capable of producing higher mechanical power. While a larger frontal area is a consequence of increased size and strength, it has a negative effect on aerodynamics and is not desirable to maximize on its own.

The first pedal stroke seems to be the dominant factor in start performance. The results revealed that 93 – 96% of the variation in start velocity could be explained by the velocity at the onset of the gate drop and the power of the first pedal stroke alone [5].

Several studies have examined the influence of bicycle components on BMX start performance. Campillo *et al.* [15] examined the effects of crank length on BMX start performance. The researchers found that the angular velocity of the crank was highest when a crank length of 182 mm was used, compared to crank lengths of 175 mm and 180 mm. The higher angular velocity resulted in a greater linear velocity. A crank length of 180 mm is mostly used in BMX racing [15].

Rylands *et al.* [16] examined the optimal gear ratio for the BMX start, using gear ratios of 41/16, 43/16, and 45/16 in a randomized order. The highest peak mechanical power and peak torque were achieved with the gear ratio 45/16, while the standard gear ratio in BMX racing is 43/16 [16]. No significant effect was observed on the time to peak power and mechanical work across the tested gear ratios. It is important to consider that optimizing crank length and gear ratios for the start should not interfere significantly with performance later in the race.

Gianikellis *et al.* [17] considered the reaction speed to the start signal to be one of the most important factors in start technique.

Additionally, the development of a robust gear-shifting system for the BMX SX start was found to hold significant potential. During the Tokyo 2020 Olympic Games, rider Twan van Gendt utilized a 2-speed gearing system to gain a competitive advantage at the start [18]. Such a system could allow riders to achieve higher velocities on the start ramp and the first straight section by enabling them to pedal at an optimal cadence of approximately 100 revolutions per minute, where BMX riders can produce higher mechanical power output [19]. After reaching the optimal cadence, the rider can shift to a higher gear ratio, maintaining high power output while increasing speed.

While a higher gear ratio and longer crank length than the standard could improve the gate start and overall BMX performance [15], [16], these recommendations are not widely adopted by riders. These changes may require slight technique adjustments, necessitating extensive training and practice.

One of the drawbacks of these experimental studies is that they were conducted with relatively small participant groups. This makes it complicated or even impossible to separate the effects of different contributing factors. Furthermore, there is limited research on the BMX start, making it difficult to compare and validate results.

Therefore, it would be of interest to have a biomechanical model and use simulations to investigate the isolated effects of factors such as different crank lengths, gear ratios, reaction times, rider strength, and coordination on start performance.

1.2. Advantages and Limitations of Biomechanical Modelling

Conducting research using biomechanical model simulations offers several advantages over experimental studies. Simulations provide a controlled environment for precise variable manipulation, improved reproducibility, and cost-effective, risk-free experimentation [20], [21]. It also gives insight into the underlying mechanics. However, it is important to acknowledge the limitations of simulations as well. Models often require approximations and assumptions, which can introduce uncertainties and reduce the accuracy of the results. Therefore, it is crucial to verify and validate models against experimental data to ensure their validity.

Once a biomechanical model is available, a particularly useful simulation tool is optimal control. Optimal control simulations find the control signals (e.g. muscle activations or joint torques) that maximize a

performance metric (e.g. velocity after 3m) for a given biomechanical model.

By varying model parameters, such as crank length or system mass, and repeating the optimal control simulation, the effects of changing these model parameters can be studied. In prior work, simulations using optimal control have been successfully applied in cycling studies to optimize pedalling techniques [22], [23] and standing track starts [20].

This thesis builds upon previous biomechanical modelling research. Groenhuis [6] developed a torque-driven BMX rider plus bicycle model in OpenSim for the BMX start, and solved an optimal control problem cast as an optimal tracking problem to verify the model. Although this model could accurately reproduce the kinematics of the BMX SX start from 0.387 s after the red start light, the recoil phase could not be reproduced by the model, which lasted until 0.37 s. Since the recoil movement is one of the most important phases [12], it is crucial to have an accurate model for this phase as well. In the study by Groenhuis [6], the recoil movement likely could not accurately be reproduced, since the experimental data of both the crank rotation and rear wheel rotation were tracked. In the model, the crank rotation was bidirectionally coupled with the rear wheel rotation, whereas in real life, they are unidirectionally coupled due to the free hub mechanism found in all BMX racing bicycles. This bidirectional coupling caused the crank and rear wheel rotations to not align during the backward movement of the bicycle in the recoil phase. Additionally, during the recoil movement, there was a period where the rear wheel slipped, causing rapid rotation of the wheel. This rapid rotation resulted in an unrealistically high crank torque in the simulation.

1.3. Research Aims

The aim of this thesis is to gain deeper insights into the mechanics of the BMX start, with the ultimate goal of optimizing performance at the start of a BMX race. Specifically, this research seeks to identify the optimal control inputs that maximize the horizontal velocity of the bicycle at the kink, using direct optimal control techniques.

Four subgoals are formulated to cover the overall research aim. For the first three goals, a simplified model of the leg-to-crank actuation is used. In this simplified model, the applied crank torque is detached from the rider and directly applied to the crank by an ideal actuator with activation dynamics. The torque is constrained to positive values to ensure that it can only produce forward propulsion of the bicycle.

GOAL 1: Adapt the model by Groenhuis [6] to enable simulation of the whole BMX start, including the recoil phase.
The first goal is to adapt the model by Groenhuis [6], to enable simulation of the recoil phase and to solve the optimal control problem of the whole BMX start until the kink. Specifically, with the objective to identify the optimal control inputs that maximize the linear velocity of the bicycle at the kink.

Goal 2: Investigate the influence of rider strength.
The second goal is to study, the influence of maximal rider strength on BMX start performance, focusing on the length of the recoil phase, timing, and kinematics. This is achieved by solving the optimal control problem for a range of maximal crank torques (250 Nm, 275 Nm, 300 Nm, 325 Nm and 350 Nm) using a simplified model.

The upper bound of the chosen range of 250 Nm to 350 Nm reflects the measured peak torque at the start for one Dutch elite female rider, for whom data was available. The crank torque follows an approximately sinusoidal function with a maximal crank torque of approximately 340 Nm, a minimal crank torque around 50Nm, and a mean torque of around 200 Nm between movement initiation and kink time at 1.2 s for this rider [6]. Since OpenSim can only model maximal crank torque as a constant, the chosen range aims to encompass the observed peak torque and lower values, providing a broad understanding of how rider strength influences BMX start kinematics and dynamics.

Goal 3: Investigate the influence of reaction time.
The third aim is to investigate the influence of reaction time on BMX start performance. This study focuses on reaction times ranging from 0.14 s to 0.18 s after the red light. This range was chosen based on data showing that the reaction time of female sprinters to an auditory signal falls between 0.14 s and 0.32 s with a 95% confidence interval [24]. The reaction time of a Dutch elite female rider,

from whom we have data available, was 0.18 s. Grigg [13] found that the reaction time of BMX riders is trainable, thus only faster reaction times were investigated. The fastest reaction time within the 95% confidence interval, 0.14 s, was chosen. The influence of reaction times of 0.14 s, 0.16 s, and 0.18 s on BMX start performance, measured in terms of kink time, horizontal velocity at the kink, at the initiation of the gate drop, and the gate drop will be investigated using optimal control by optimizing the linear bicycle velocity.

We hypothesize that the reaction time will have a significant effect on the optimal start technique in BMX racing. Specifically, we expect that a faster reaction time leads to a greater recoil. Given the variability in reaction times, we believe it might be more effective to consistently use a strategy optimized for a slower, more reliable reaction time (e.g., 0.18 s), rather than attempting to achieve a faster reaction time with higher variability and potentially employing a suboptimal technique.

Goal 4: Implement and verify a complete torque driven model to better represent the torque at the crank.
The final goal is to implement and verify/validate a complete torque driven BMX rider plus bicycle model. This will be achieved by using a comprehensive model of the BMX rider and bicycle that includes the entire body of the rider, with the assumption of one arm having twice the strength due to symmetrical movement. This model, based on the work by Groenhuis [6], aims to better replicate the torque at the cranks by accurately representing the rider's biomechanics. This model will be validated with an optimal control problem cast as an optimal tracking problem, where the objective is to find the control inputs that minimize the error between the model's output and the experimentally measured kinematics of the BMX start. This approach is used to validate the model by demonstrating that it can follow known trajectories or behaviours accurately, which in turn suggests that the model is realistic and reliable. The produced torque at the cranks will then be compared to the experimentally measured torque at the crank.

Also, a predictive optimal control problem will be solved with this model to gain insight into the optimal kinematics and dynamics of the BMX start.

2

Theoretical Background

This chapter provides a comprehensive overview of the theoretical foundations pertinent to the optimal control problem and the numerical optimization methods employed to solve them. Specifically, it focuses on two prominent approaches: Direct Collocation and Single Shooting, highlighting their methodologies and ideal use cases. Furthermore, the chapter discusses software toolkits available for OpenSim, such as Scone and Moco, and delves into the transcription schemes and numerical solvers used to solve optimal control problems.

2.1. Optimal Control Problem

Optimal control theory provides a mathematical framework for determining the optimal control inputs over time that minimize or maximize a specific objective function, subject to constraints on the system's dynamics, state variables, and control inputs. This section examines two prominent numerical optimization methods within this domain: Single Shooting and Direct Collocation. Both are crucial for addressing optimal control problems, but they differ in their methodologies and ideal use cases.

For OpenSim, two software toolkits are available: Scone and Moco. Scone is built on top of OpenSim and enables researchers to use shooting methods to solve optimization problems [25]. Moco, short for Musculoskeletal Optimal Control, uses direct collocation, which is often faster, to solve trajectory optimization problems with models defined in OpenSim [26]. Shooting methods and direct collocation serve as fundamental tools for solving optimal control problems, each possessing unique characteristics that make them suitable for specific applications. This section delves into the differences between these two approaches, highlighting their discretization strategies and computational implications.

2.1.1. Single Shooting

In contrast, Single Shooting employs a single set of decision variables for the entire trajectory. This method is conceptually simpler and is preferred when the system dynamics are straightforward and computational efficiency is a priority

Discretization Strategy:
In Single Shooting, the entire time horizon is represented by one set of decision variables. While computationally efficient, it may not capture highly complex dynamics as effectively. It suits scenarios where computational resources are limited, and the system dynamics exhibit a degree of linearity.

2.1.2. Direct Collocation

Direct Collocation is a robust numerical optimization technique widely used for solving optimal control problems with continuous-time dynamics. It models the evolution of system dynamics over a finite time horizon by discretizing it and treating the state and control trajectories as piecewise continuous functions. This method is particularly advantageous for systems with complex and nonlinear dynamics, making it applicable across fields such as biomechanics, aerospace, and robotics.

Discretization Strategy

Direct Collocation breaks the time horizon into intervals, associating decision variables with each interval. These variables represent the state and control trajectories within each interval, ensuring a comprehensive depiction of the system's behaviour. The approach minimizes a cost function subject to discretized dynamics, incorporating both state and control constraints. Its capability to manage complex dynamics and constraints underpins its suitability for a wide range of applications.

2.1.3. Moco

Moco provides pre-built optimization goals, such as motion tracking, parameter optimization, minimizing control effort and optimizing a final output [26].

By considering of factors like muscle activations, joint angles, and external forces to optimize the movement, aligning with desired objectives or constraints enables Moco to optimize movement in alignment with specified objectives or constraints. Users specify their goals, such as minimizing control effort or achieving a specific motion pattern, and Moco processes this information to determine optimal control signals for the system.

In essence, Moco is a valuable resource for those exploring optimal control within the domains of human and biomechanical movement, simplifying the process of finding the most efficient and effective motion patterns for different applications.

2.1.4. Hermite-Simpson Transcription Scheme

The transcription of the continuous-time optimal control problem into a discrete-time problem can be done with either a trapezoidal scheme or the Hermite-Simpson transcription scheme. The Hermite-Simpson transcription scheme approximates the trajectory of the system's state and control variables by discretizing the time horizon into multiple intervals and using polynomial interpolation to ensure smoothness and accuracy.

The Hermite-Simpson transcription scheme involves dividing the time horizon into intervals, with each interval defined by time points. Within each interval, the states, and controls are approximated using cubic Hermite polynomials, which can represent both the value and the derivative (slope) of the state variables at the endpoints of the interval [27]. Additional collocation points are introduced at the midpoints of each interval to enforce the system's dynamics more accurately. The dynamic equations of the system are enforced at both the interval endpoints and the collocation points, ensuring the differential equations are satisfied over the entire interval. The Hermite-Simpson scheme minimizes discretization error by ensuring continuous and well-approximated state and derivative trajectories, resulting in a more accurate and stable solution.

The trapezoidal scheme approximates the state and control trajectories using linear interpolation, which can result in higher discretization errors and less smooth solutions (Figure 2.1.1). While the trapezoidal scheme is computationally simpler and faster, it may not capture the intricate dynamics of nonlinear systems as effectively as the Hermite-Simpson scheme. Compared to the trapezoidal scheme, the Hermite-Simpson scheme offers greater accuracy and stability for complex systems.

Nonlinear program

After transcription, the discrete-time problem is then converted into a finite-dimensional nonlinear program (NLP). This involves setting up the objective function and constraints in a form that can be solved by a numerical optimizer. Moco employs numerical solvers to solve the NLP. The primary solver used by Moco is Interior Point OPTimizer (IPOPT), an open-source software package for large-scale nonlinear optimization [28].

2.1.5. Interior Point OPTimizer

IPOPT takes the finite-dimensional nonlinear program (NLP) formulated by Moco and begins the optimization process. This process starts with initialization, where IPOPT begins with an initial guess for the state and control variables. The next phase is iteration. IPOPT iteratively improves the solution by solving a series of linearized sub-problems. In each iteration, it updates the state and control variables to reduce the objective function while ensuring that the constraints are satisfied. To handle inequality constraints, IPOPT employs a barrier function. This function penalizes solutions that approach the

boundary of the feasible region, thus ensuring that the iterations remain within the feasible region.

IPOPT continues iterating until the convergence criteria are met. These criteria include a specified tolerance for the objective function improvement, satisfaction of the constraints, and the size of the step taken in each iteration. Once IPOPT converges, it provides the optimized state and control trajectories that minimize the specified objective function.

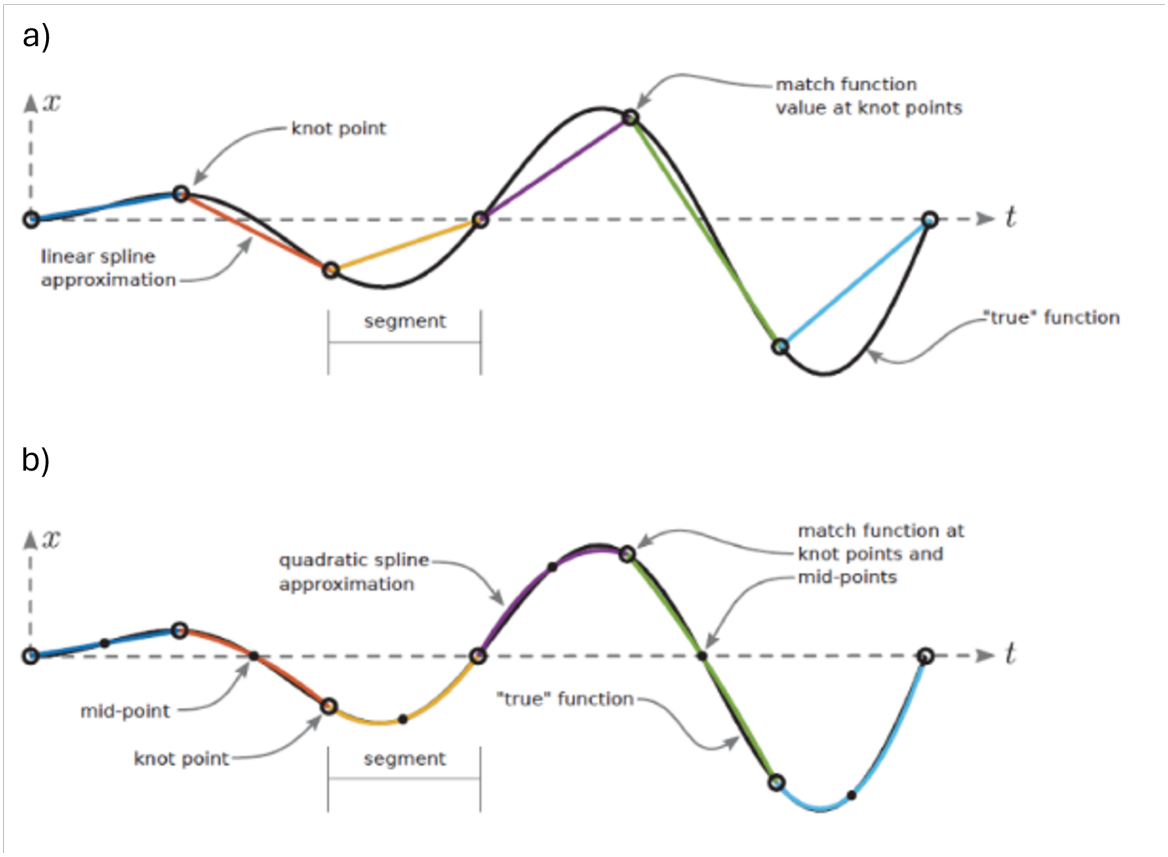

Figure 2.1.1: Comparison Between Trapezoidal (a) and Hermite-Simpson (b) Transcription Scheme. This figure compares the Trapezoidal and Hermite-Simpson transcription schemes used in numerical methods. Adopted from Kelly [27].

3

Method

This chapter discusses the two BMX rider plus bicycle models used. And the formulation of the optimal control problem.

This chapter discusses the two BMX bicycle-plus-rider models used in this study and the formulation of the optimal control problem. It details the development and validation of the models, the components, and setup of the optimal control problem, and the simulation scenarios designed to achieve the research goals.

3.1. BMX Rider Plus Bicycle Model

3.1.1. Previous BMX Model Development

The BMX rider plus bicycle model is based on the foundational work by Groenhuis [6], who created a BMX rider plus bicycle model for the start phase and validated it using a tracking optimization approach. This approach aimed to find the optimal set of control inputs that minimize the difference between the experimentally measured joint angles and the simulated joint angles of the model. This model was valid for the forward pedalling motion that starts after the recoil phase. The model was created in OpenSim, an open-source software package for biomechanical modelling [29], [30]. The thesis of Groenhuis [6] provides details regarding the parameter determination of both the bicycle and the rider, including mass, inertia, centre of mass, and more.

The optimal tracking simulation results demonstrated close alignment with experimental kinematic data from 0.387 s to 1.504 s after the red starting light. An average root mean squared error (RMSE) of 0.38° was found for the six joints of the legs between the optimized tracking simulation and the experimental kinematic data. The tracking of crank angle and horizontal displacement of the bicycle yielded comparable results, with RMSEs of 0.34° and 0.038 m respectively. The RMSE between the experimentally measured net torque and net power, which were not tracked, was 56.36 Nm and 1072.17 W, respectively.

However, the model was not valid for the recoil motion due to the lack of a free hub in the model. One reason for this was that in the model, the rear wheel is connected with a bi-directional coordinate coupler between the crankshaft and the rear wheel. Due to this coupler, the rider could pedal backward to drive the rear wheel and thus move the bicycle backward. In real life, this is not possible with a bicycle with a free hub like a BMX bicycle and most other bicycles.

A bicycle with a free hub can only move backward when the centre of mass is shifted forward (on a level surface) due to the conservation of momentum. This backward motion cannot be achieved by applying negative propulsive force (i.e., pedalling backward) because the free hub mechanism prevents it. To address this, the leg-to-crank actuation will be simplified by directly actuating the crank and constraining the crank torque to only positive values in a simplified model with only the upper body and bicycle. This ensures that the backward pedalling issue is avoided in the simulation.

Another reason was that in the kinematic data, which was used to validate the model, there was a moment where the rear wheel slipped relative to the ground in all recorded trials. The rear wheel in the OpenSim model cannot slip, due to the determined contact parameters. This caused trouble with the optimal tracking simulation, where the objective was to match the states of the model with the measured kinematics to validate the model. Allowing rear wheel slip in the model would make the model more complex and require extensive knowledge of tyre and contact dynamics, so in this study the same contact parameters between the ground and rear wheel which allow no slip will be used as in the study by Groenhuis [6].

This section will discuss the two BMX rider plus bicycle models used in the optimizations.

3.1.2. Current BMX Model

The BMX plus rider is modelled as a planar system to reduce complexity. Allowing lateral movement and the roll angle of the bicycle would significantly increase the model's complexity. Since BMX riders are skilled in balancing the bicycle, adding the roll angle would likely not influence the optimal control solution. The start of the BMX race is mostly in a straight line and depends on the opponents, which cannot be modelled. Therefore, adding a steer would unnecessarily complicate the model, so the steer is welded to the bicycle frame.

Two models have been created. The first model, the 'Upper Body Model', is a simplified version of the original BMX model by Groenhuis [6] with only the BMX bicycle, the upper extremities and the torso (Figure 3.1.3.a). This model could better replicate the recoil movement by bounding the torque at the cranks to only positive values.

The second model, the 'Full Body Model' is an improved version of the BMX model created by Groenhuis [6] (Figure 3.1.3.b). This model produces a more realistic torques at the cranks since this torque is produced by the torque around the hip, knee, and ankle joints. In this model, a top and bottom dead centre can be seen in the torque curve. This model has 11 degrees of freedom (DOF), making the predictive optimal control simulation with this model computationally expensive.

3.1.3. Bicycle

The bicycle consists of four rigid bodies: the bicycle frame (including the steer), two wheels and the crankshaft. The wheels and crankshaft are connected to the bicycle with a pin joint. The rotation of the cranks is coupled with the rotation of the rear wheel with a coordinate coupler constraint. The *CoordinateCouplerConstraint* in OpenSim couples two coordinates with a user-defined function. In this case, the rear wheel rotates 2.75 times the rotation of the crankshaft. 2.75 represents the gear ratio, which is the number of teeth of the chainring divided by the number of teeth of the sprocket. The chainring of the bicycle used during the measurements of the experimental kinematics had 44 teeth and the sprocket 16.

The dimensions of the bicycle frame and wheels in the model are detailed in Figure 3.1.2). The mass and inertia of all bodies in the model can be found in table 3.1.1. Groenhuis [6] describes how these parameters were determined.

The opening of the gate is modelled using a prescribed step function, set to open from 90 degrees to zero degrees between 0.36 s and 0.67 s, as displayed in Figure 1.1.2. This step function closely matches the measured gate angle at the start and finish times. The measurements were obtained using Kinovea to track the x and y positions of a point on the gate. In the middle of the opening interval, the maximum deviation is approximately 10 degrees. The experimentally measured gate angle and the modelled gate angle and angular velocity can be seen in Figure 3.1.1.

3.1.4. Rider

The model for the BMX rider is based on the generic model *gait10dof18musc*, which, as the name suggests, has 10 degrees of freedom (DOF) and 18 muscles. It was developed to analyse human gait [31]. This planar model features all human joints modelled as one DOF joints and includes only the lower body and trunk. The arm from the *arm26* [32] OpenSim model is used to represent the right arm of the body. Only one arm is modelled, with twice the weight and strength to account for symmetrical right and left arm movements. The skeletal dimensions come from these two models. The length of

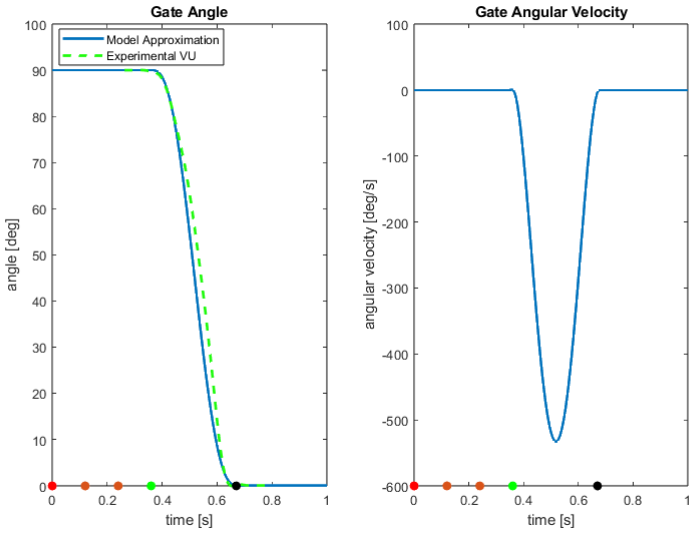

Figure 3.1.1: Measured Gate Angle from Video Footage Using Kinovea and Modelled Gate Angle and Angular Velocity Using OpenSim. The figure shows the comparison between the gate angle measured from video footage using Kinovea and the gate angle modelled in OpenSim. In the OpenSim model, the gate angle is defined using a step function, transitioning from 90 ° at 0.36 s to 0° at 0.67 s.

the rider from whom we have experimental data available was 2 cm smaller compared to the length of the human in the *gait10dof18musc* model. The dimensions of all segments can be found in Table 3.1.1.

Simplified Upper Body Model

To address the challenge of modelling a free hub and to reduce the degrees of freedom (DOF) to minimize computational time during optimization, a BMX model featuring only the upper body and the bicycle was developed. This model will be used for the first three research goals.

A coordinate actuator at the crankshaft was added to the model to simulate leg actuation, with a maximum torque of 300 Nm. This value was determined based on the maximal measured crank torque by Grieken [33] (Figure 4.2.5).

The normalized torque at the crankshaft was constrained between 0 and 1 to prevent negative torque during the simulation of the predictive optimal control problem for the recoil phase, ensuring the bicycle could only move backward by shifting the centre of mass forward. The mass of the legs and pelvis was integrated into the torso.

The torso at L5, was connected to the bicycle frame using an OpenSim custom joint, positioned 0.55 m above the rear wheel hub. This custom joint permits horizontal translation along the x-axis of the bicycle (torso horizontal translation) and rotation around the z-axis (torso lean angle). To further decrease computational time, no movement in the y-direction was defined for the custom joint. The number of DOF was reduced from 11 in the 'Full Body Model' to six in the 'Upper Body Model'.

The DOF can be calculated with the Kutzbach equation for a planar system (Equation 3.1) [34]. This is given by:

$$M = 3(N-1) - 2L_P - H_P \tag{3.1}$$

Here, M is the DOF of the mechanism (Mobility), N represents the total number of links in the mechanism including a ground or fixed link, L_P represents the number of lower pairs (joints with one DOF), and H_P represents the number of higher pairs (joints with two DOF).

Firstly, there are four DOF for the bicycle: frame horizontal translation, frame pitch angle, one for the crankshaft rotation, and one for the front wheel rotation of the bicycle. The rear wheel has no DOF since it is coupled with the crankshaft.

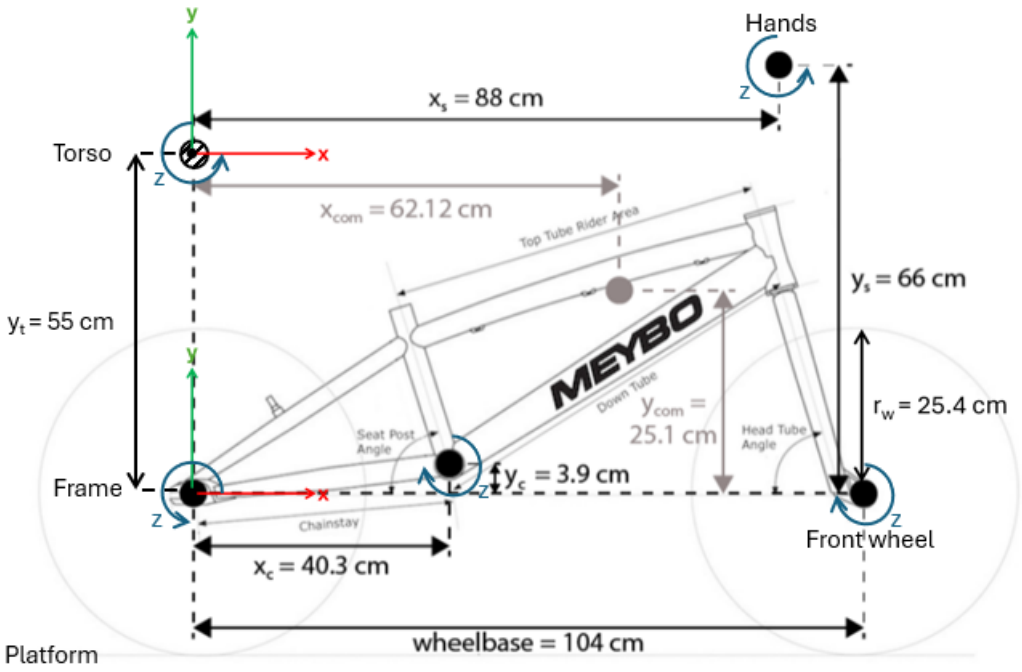

Figure 3.1.2: Dimensions of the BMX Used in the Models. The grey dot represents the centre of mass of the BMX. The black dots indicate the connection points of the wheels, crankshaft, and hands. The striped dot represents the connection point of the torso at L5 (only present in the 'Upper Body Model'). The axes at the torso and frame connection points illustrate the movement directions of the torso and bicycle frame joints. The torso can translate horizontally along the x-axis, and the lean angle is defined around the z-axis. The bicycle frame can also translate horizontally along the x-axis, with the pitch angle defined around the z-axis. 'c' stands for chain stay, 's' for hands, 'rw' for the radius of the wheels, and 't' for torso. Adapted from Groenhuis [6].

Secondly, there are two DOF for the upper body. The upper body consists of a torso that can translate horizontally in the x-direction and rotate around the z-axis (the torso lean angle) (Figure 3.1.2), and a pin joint for the shoulder and elbow flexion. The hand is connected with a Point-on-Line Constraint rather than a pin joint, to avoid a closed kinematic chain (Figure 3.1.3). The number DOF is determined using Equation 3.1. The number of links of the upper body is four (lower arm, upper arm, torso and 'ground' link), the number of lower pairs is three (hand, elbow, and shoulder joint) and the number of higher pairs is one (torso joint), this gives a DOF of two using Equation 3.1.This makes a total of six DOF for the whole bicycle rider system of the 'Upper Body Model'.

Connection with the Bicycle The rider needs to be connected with the bicycle, but a closed kinematic chain should be avoided. To avoid a closed-loop kinematic chain, the hand is connected with a Point-on-Line Constraint to the handlebar instead of a joint. A Point-on-Line Constraint instead of a Point constraint was used to avoid an assembly tolerance issue in OpenSim. The torso at L5 is connected to the bicycle frame using an OpenSim custom joint, allowing horizontal translation and rotation around the z-axis.

Full Body Model

The 'Full Body Model' (Figure 3.1.3.b) is very similar to the model used by Groenhuis [6], but the damping of the joints is decreased, the opening of the gate is differently defined (the gate angle coordinate is prescribed by a step function, instead of prescribing the torque needed for the opening), contact forces are added between the front wheel and gate, and the sphere shaped meshes for the arm are replaced by meshes representing the bones.

The system has 11 degrees of freedom (DOF). Firstly, the bicycle has the same four DOF as the bicycle in the 'Upper Body Model'.

For the rider, the number of degrees of freedom is seven. The number of links is 10 (lower arm, upper arm, torso, two upper legs, two lower legs, two feet, and 'ground' link), $L_p = 10$ (hand, elbow, shoulder,

Body	Mass (kg)	Inertia (kg·m^2) [Ixx Iyy Izz Ixy Ixz Iyz]	Centre of Mass (m) [x y z]
Bicycle frame	5.2	[1 1 0.79 0 0 0]	[0.621 0.251 0]
Front wheel	1.28	[1 0.062 1 0 0 0]	[0 0 0]
Rear wheel	1.579	[1 0.076 1 0 0 0]	[0 0 0]
Crankshaft	0.98	[1 0.014 1 0 0 0]	[0 0 0]
Torso*	61.18	[1.475 0.756 1.431 0 0 0]	[0.010 −0.28 0]
Humerus	4.06	[0.015 0.005 0.013 0 0 0]	[0 −0.015 0]
Ulna & radius	3.4	[0.019 0.002 0.020 0 0 0]	[0 −0.181 0]
Gate	100	[4.167 2.097 2.097 0 0 0]	[0 0 0]
Platform	1	[1 1 1 0 0 0]	[0 0 0]
Torso**	20.24	[1.4745 0.7555 1.4314 0 0 0]	[−0.05 −0.1 0]
Pelvis**	11.78	[0.103 0.087 0.058 0 0 0]	[−0.071 0 0]
Femur**	9.3	[0.134 0.035 0.141 0 0 0]	[0 −0.17 0]
Tibia**	3.71	[0.050 0.005 0.051 0 0 0]	[0 −0.187 0]
Talus**	0.1	[0.001 0.001 0.001 0 0 0]	[0 0 0]
Calc**	1.25	[0.001 0.004 0.004 0 0 0]	[0.1 0.03 0]
Toes**	0.22	[0.000 0.000 0.000 0 0 0]	[0.035 0.006 −0.018]

Table 3.1.1: Information on All Bodies in the OpenSim BMX Model. The inertia is measured around the centre of mass. The centre of mass is in the body frame. * Denotes bodies only present in the 'Upper Body Model'. **Denotes bodies only present in the 'Full Body Model'.

two hips, two knees, and two ankles joints) and $H_P = 0$, this make a DOF of 7 using 3.1. This makes a total of 11 DOF for the 'Full Body Model'.

Connection with the Bicycle The rider needs to be connected with the bicycle, but a closed kinematic chain should be avoided. To avoid a closed-loop kinematic chain, the hand is connected with a pin joint and both feet with a Point-on-Line Constraint instead of a joint. The feet are connected with a constraint because they are connected with a clip system in real life, and the wrist could exert a small torque in real life. Closed-loop kinematic chains can lead to difficulties in deriving equations of motion in terms of generalized coordinates, and they could lead to singularity, making it challenging to optimize the system. A Point-on-Line Constraint instead of a Point Constraint was used in OpenSim to avoid an assembly tolerance issue.

3.1.5. Forces

Activation Coordinate Actuators

The foundational models (*gait10dof18musc* and *arm26*), contain muscles to actuate the model using forward dynamics. They explicitly simulate the dynamics of muscles and tendons to drive the musculoskeletal model. These models produce physiologically accurate movements, However, this approach is computationally expensive for predictive optimal control simulations due to the increased number of state variables. Multiple muscles generate torque around the joints, and every modelled muscle has two state variables, namely the muscle activation, and fibre length. Because of the computational expense, the muscles were removed from the models and replaced with ideal actuators with activation dynamics at all joints to represent the net forces delivered by the muscles around a joint. Although these actuators lack the dynamics of muscles, such as the force-length [35] and force-velocity relationships [36], they have been successfully implemented in predictive simulation studies on human movement and sports applications [23], [37]–[39].

The ideal actuators with activation dynamics are implemented in OpenSim using the *ActivationCoordinateActuator*[1] class in OpenSim. Activation dynamics are modelled as first-order linear dynamics, described by the equation $\dot{a} = \frac{x-a}{\tau}$ where a represents activation, x denotes excitation or control value, and τ is the activation time constant. The activation time constant accounts for the delay in muscle activation due to physiological processes such as calcium ion release and reuptake in the sarcoplasmic reticulum, which control the contraction and relaxation phases of the muscle [40].

[1] `https://simtk.org/api_docs/opensim/api_docs/classOpenSim_1_1ActivationCoordinateActuator.html`

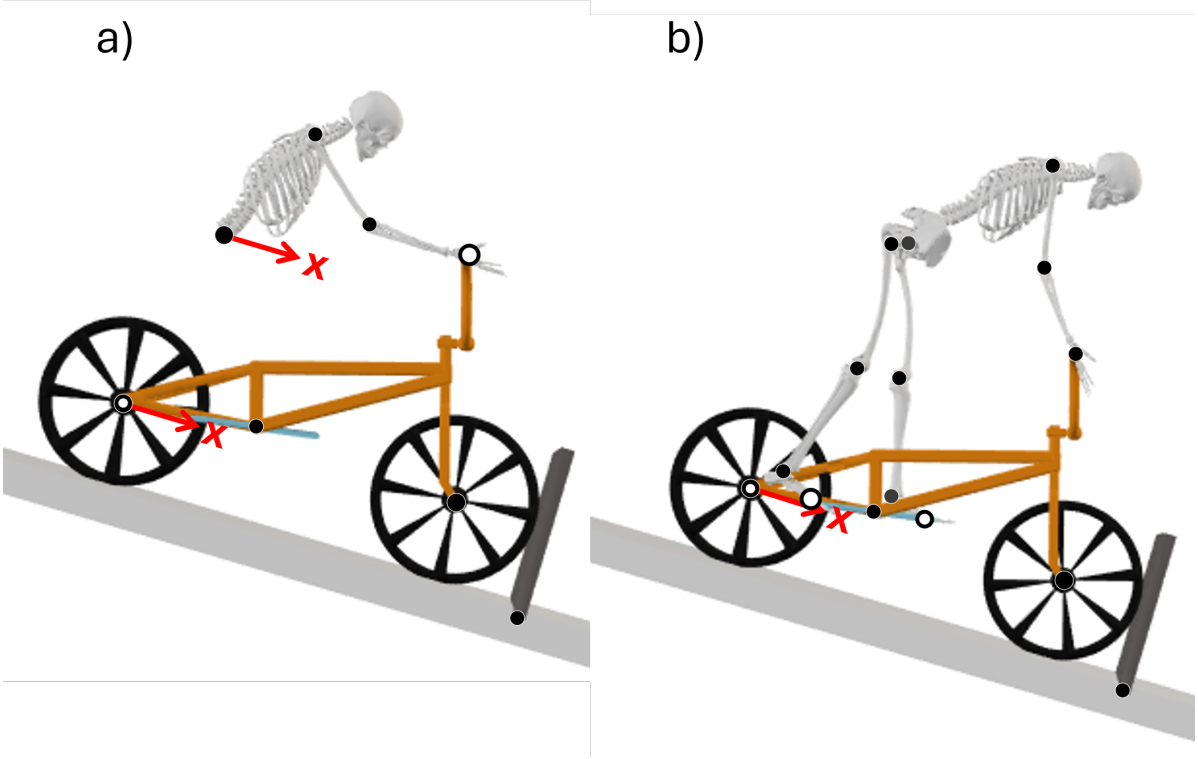

Figure 3.1.3: 'Upper Body Model' (a) and 'Full Body Model' (b).These models are planar torque drive models in the y-x plane. All black dots are 1 degree of freedom rotational joints. The torso is connected to the bicycle frame above the rear wheel hub. The torso can rotate (torso lean angle) and translate in the x direction in the 'Upper Body Model' (a). The white dots are constraints. There are point-on-line constraints at the hand for the 'Upper Body Model' and both feet in the 'Full Body Model'. At the location of the rear wheel hub is a constraint and joint. The rotation of the rear wheel is constrained by the coupling between the rotation of the cranks and the rotation of the rear wheel. The bicycle can translate horizontally in the x direction and rotate around the rear wheel hub (bicycle pitch angle). The bicycle is clamped to the ramp (no translation in the y direction).

A typical activation time constant for muscle activation ranges from 0.005 s to 0.05 s, depending on the muscle type (like fast-twitch and slow-twitch fibres) and conditions [41]. The deactivation time constant in muscles is usually slightly longer than the activation time constant, because the calcium reuptake is slower, ranging from 0.02 to 0.05 s. In the model, only the same value for the activation and deactivation constant can be set. All actuators have an activation and deactivation time constant of 0.03 s in the models. This relatively short time constant was chosen because BMX racing is a sprint discipline, so riders likely primarily rely on fast-twitch muscle fibres, which are suited for rapid and powerful movements typical in sprint disciplines. Fast-twitch fibres have quicker activation dynamics, making a 30-millisecond time constant appropriate for simulating BMX performance.

The minimal control value is -1 and the maximal control value is 1 for all actuators, except for the crankshaft. The control value for the crankshaft ranges between 0 and 1 to prohibit negative torque, ensuring the bicycle cannot be propelled backward by pedalling backward.

The maximal force for the translational coordinates and the maximal torques for the rotational coordinates can be found in Table 3.1.2.

Limit Forces

All joints with an actuator, except the joint at the crankshaft, have a limit force acting on the joint when either the upper or lower joint limits are exceeded (Table 3.1.2). These limit forces simulate the natural constraints imposed by ligaments and other passive tissues, which prevent the joints from moving beyond their physiological range of motion. The upper and lower stiffness when the limits are exceeded are set to 50 N/m for the translational coordinate of the Torso and 50 N*m/degree for the rotational coordinates. The damping when the coordinate is exceeded is 0.025 (for translational coordinates in N/(m/s) and rotational coordinates in Nm/(degree/s). The transition region, which determines the

Joint	Maximal Force/Torque	Lower Limit	Upper Limit
Torso Horizontal Translation*	600 N	0 m	0.85 m
Torso Lean Angle*	600 Nm	-45°	45°
Crankshaft Rotational Angle*	300 Nm	-280°	1430°
Shoulder Flexion	400 Nm	-90°	180°
Elbow Flexion	250 Nm	0°	130°
Hip Flexion**	400 Nm	-30°	120°
Knee Flexion**	300 Nm	-120°	10°
Ankle Flexion**	250 Nm	-45°	45°
Hand Flexion**	50 Nm	-90°	0°

Table 3.1.2: Joint Information and Maximal Joint Torques/Forces. This table details the joint limits of the ActivationCoordinateActuators. * Denotes ActivationCoordinateActuators only present in the 'Upper Body Model'. ** Denotes ActivationCoordinateActuators only present in the 'Full Body Model'.

shift from zero to a constant stiffness when the coordinate exceeds its limit, is 5 degrees for rotational coordinates or 0.05 m for translational coordinates.

Damping

To stabilize the system and prevent oscillations, damping is added to the coordinates of the rider with a damping coefficient of 6.25 N·m/rad·s for the upper extremities, and the torso coordinates. The lower extremities have a damping coefficient of 2.5 N·m/rad·s. This is implemented in the OpenSim model with a *SpringGeneralizedForce* [2]

Contact Forces

Contact modelling plays a critical role in simulating the interaction between the wheels and the ground. The ability of the bicycle to propel itself forward relies heavily on how accurately these interactions are modelled.

Contact forces between both wheels and the platform, as well as between the front wheel and gate, are modelled. The contact modelling of the front wheel and rear wheel follows the methods described in Groenhuis [6]. The contact force between the wheels and the platform is modelled with a Hunt-Crossley force. This is based on Hertz contact theory, which describes the interaction between two elastic bodies under load. This section provides a broad overview of the contact forces. A more elaborate explanation of the determination of the contact parameters can be found in the thesis by Groenhuis [6].

Contact Geometries Before defining the contact forces, it is necessary to define the contact geometries. In OpenSim there is the choice between a *ContactSphere* [3], *ContactHalfSpace*[4] and *ContactMesh* [5]. A *ContactMesh* allows all surfaces to be represented with a mesh grid. However, the contact forces between such a mesh grid and another contact geometry can only be calculated using an Elastic Foundation model. This approach is computationally intensive, as it requires calculating the interaction forces at every mesh centre, represented by tiny springs.

Firstly, a contact plane is connected on top of the surface of the platform with a slope of 16.5 degrees. The slope of the platform of the BMX SX start ramp is not constant, this is implemented in OpenSim with a *ContactHalfSpace* (Figure 3.1.4). From the gate until 4 m behind the gate the slope is 15 degrees, and from the gate until the kink at 3.15 m the slope is 18 degrees. At the kink, the slope sharply changes to 28 degrees. In this study we are dominantly interested in the optimization of the start until the kink; therefore, it has been chosen to model the ramp at a constant angle of 16.5 degrees which is the mean angle of the platform behind the gate and until the kink. A step-wise increasing slope of the platform would not work since the contact planes would intersect. The contact of the platform could be modelled with a contact mesh, but this would be a lot more computationally expensive. Next, the contact geometry of the wheels are modelled with a *ContactSphere* [6] connected with the wheels, with

[2] https://simtk.org/api_docs/opensim/api_docs/classOpenSim_1_1SpringGeneralizedForce.html
[3] https://simtk.org/api_docs/opensim/api_docs/classOpenSim_1_1ContactSphere.html
[4] https://simtk.org/api_docs/opensim/api_docs/classOpenSim_1_1ContactHalfSpace.html
[5] https://simtk.org/api_docs/opensim/api_docs/classOpenSim_1_1ContactMesh.html
[6] https://simtk.org/api_docs/opensim/api_docs/classOpenSim_1_1ContactSphere.html

the same radius as the wheels (25.4 cm)(Figure 3.1.2). This can be done since the BMX model is a planar model. Lastly, the contact geometry of the gate is modelled with a *ContactMesh*, with the same dimensions as the gate, allowing the front wheel to lift over the gate. A contact plane would restrict this. The contact mesh of the gate is connected to the gate, with its pivot point 2 cm below the platform. When the gate is open, no forces can be exerted between the contact mesh of the gate and the front wheel since the contact plane of the platform is above the contact plane of the gate.

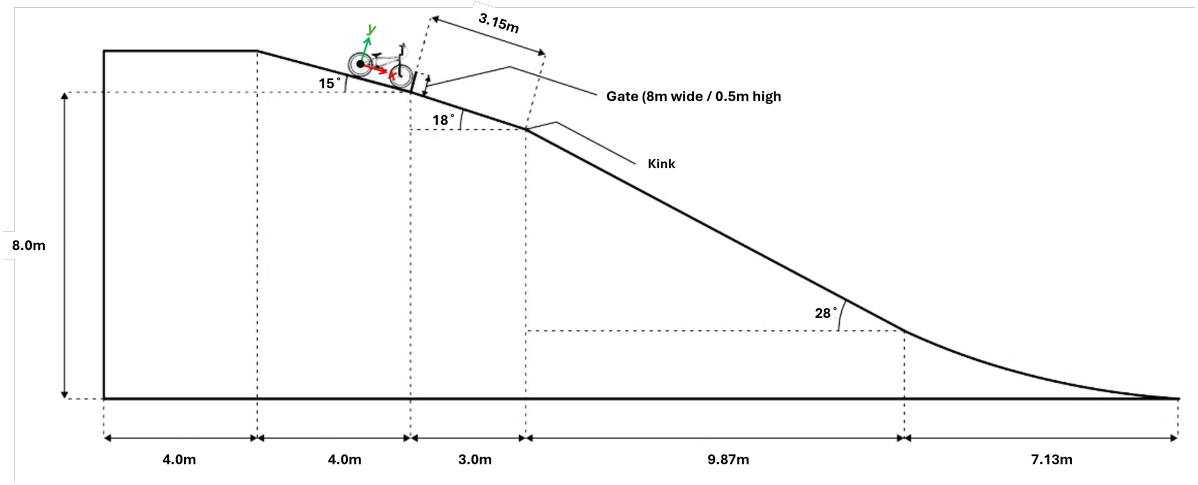

Figure 3.1.4: BMX SX Start Ramp Dimensions as Defined by UCI BMX Regulations[4]. Adapted from Grigg [13]

Contact Forces Rear Wheel The contact with the ground and the platform is modelled with a *HuntCrossleyForce* [7]. This contact model has been chosen over the Elastic Foundation model due to the smaller computational costs. More about the Elastic Foundation model can be found in the paragraph about the contact forces at the gate. The Hunt Crossley contact model is based on Hertz contact theory, which describes the interaction between two elastic bodies under load. The Hunt-Crossley model calculates contact forces by considering the elastic properties of the materials in contact, the depth of penetration, and the relative velocity at which the surfaces are moving. These factors influence the normal force, which is the force perpendicular to the contact surface, as well as the frictional forces parallel to the surface. The penetration depth is kept constant at 1 mm, simplifying the equation for the normal force component of the contact force to:

$$F_n = kx_n \tag{3.2}$$

Where k is the stiffness depending on the material and geometry ($1 * 10^7 N/m^2$ in this case), x the penetration depth (3 mm), and n is dependent on the surface and contact geometry (3/4 for a sphere and plane contact).

The frictional force component of the contact force is calculated in OpenSim, based on a model by Michael Hollars [42], with the following equation:

$$F_f = F_n \left[\min\left(\frac{v_s}{v_t}, 1\right) \left(\mu_d + \frac{2\left(\mu_s - \mu_d\right)}{1 + \left(\frac{v_s}{v_t}\right)^2} \right) + k_v v_s \right] \tag{3.3}$$

Where Fn is the normal force (Equation 3.2), v_t the transition velocity, v_s is the slip (tangential) velocity, and μ_s, μ_d and k_v the coefficients of static, dynamic, and viscous friction, respectively, all equalled to one. These contact parameters are determined experimentally with a rolling test [6]. The dissipation coefficient is set to 0.008 based on a bouncing test.

[7] https://simtk.org/api_docs/opensim/api_docs/classOpenSim_1_1HuntCrossleyForce.html

Contact Forces Front Wheel The contact between the front wheel and the platform is modelled with a *SmoothSphereHalfSpaceForce*[8] instead of a Hunt-Crossley force in OpenSim. A *SmoothSphereHalf-SpaceForce* smoothens the transition between contact and no contact and remains very small instead of zero when there is no contact. This smooth transition helps avoid discontinuities in contact force when the front wheel is lifted from the ground, which could complicate the gradient-based optimization used by Moco.

Contact Forces Gate In the simulation scenario involving contact between the gate and the front wheel, a contact force is implemented to model their interaction. The choice of using an *ElasticFoundation-Force* [9] is motivated by the ability to select a contact mesh, allowing for more realistic representation of the gate's shape. This is essential for solving the optimal control problem where the front wheel needs to be able to lift over the gate. Using a contact plane would disable this due to its infinite nature.

The Elastic Foundation model represents contact surfaces as a layer of discrete springs atop a rigid base. These springs deform elastically under pressure, with the stiffness of each spring reflecting the material properties of the contacting surfaces. When meshes collide, the displaced springs contribute to the calculation of various components, including the normal force, restoring force, dissipation in the material, and surface friction. The friction force calculation follows the same approach as the Hunt-Crossley contact model (Equation 3.3).

One drawback of the Elastic Foundation model is its computational cost. Unlike the Hunt-Crossley contact model, where forces are calculated for the entire deformed object, the Elastic Foundation model requires individual force calculations for each displaced spring. This increased computational cost should be considered when selecting the appropriate contact model for a simulation scenario.

Overall, while the Elastic Foundation model offers advantages in terms of realism and flexibility, it comes with the trade-off of increased computational complexity compared to simpler contact models like the Hunt-Crossley model. Hence, the choice to only model the contact between the gate and front wheel with the Elastic Foundation model and not the contact between the wheels and platform.

3.2. Optimal Control Problem Formulation for the BMX Start

This chapter outlines the formulation of the optimal control problem for the BMX start using the Moco software package built on OpenSim [26]. Moco uses direct collocation to solve the optimal control problem.

The problem is defined within the *MocoProblem* class, while the numerical methods to solve it are encapsulated in the *MocoSolver* class. Both classes are part of the overarching *MocoStudy* class (Figure 3.2.1). The *MocoStudy* is typically described in an XML file, detailing the problem and the numerical methods applied. The complete Moco Study for BMX optimization can be found in Appendix B. Key parameters are also discussed in the next section.

MocoProblem

The *MocoProblem* class is part of the *MocoStudy*. This class can include cost terms, a comprehensive model with multibody dynamics, muscle dynamics, kinematic constraints, boundary constraints, path constraints, parameter optimization, bounds on variables, and dynamically-constrained inverse kinematics (Figure 3.2.1).

This section outlines the components used in the MocoStudy for the BMX start, aiming to achieve the highest linear velocity at approximately the kink, located 3.15 m past the gate.

3.2.1. Objective Functions

For the whole BMX start, the nominal objective function consists of maximizing the magnitude of the linear velocity of the bicycle frame, maximizing the final position of the bicycle frame, minimizing the bicycle frame pitch angle, and slightly minimizing control effort.

[8] https://simtk.org/api_docs/opensim/api_docs/classOpenSim_1_1SmoothSphereHalfSpaceForce.html
[9] https://simtk.org/api_docs/opensim/api_docs/classOpenSim_1_1ElasticFoundationForce.html

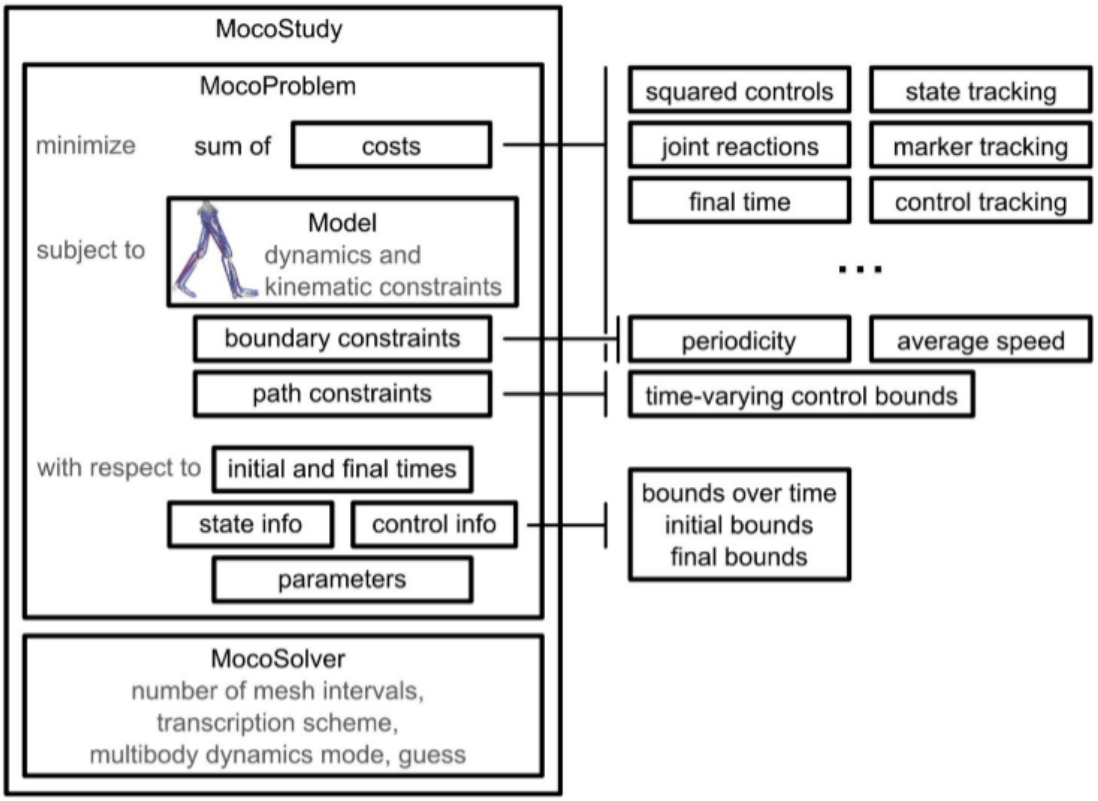

Figure 3.2.1: Components of a MocoStudy. This diagram illustrates the structure of a MocoStudy. The MocoProblem class defines the problem with elements like cost terms, multibody dynamics, and kinematic constraints. The MocoSolver class encapsulates the numerical methods to solve the problem. Adapted from Dembia *et al.* [26].

Optimizing Bicycle Position

The `MocoFinalOutputGoal` is used to optimize the final bicycle position in Moco. It is a goal used for minimizing or constraining a specific model output at the end of a trajectory.

Due to limitations in optimizing state variables in Moco, the magnitude of the position of the offset frame of the bicycle body at the front hub is optimized. This approach is used because the pitch angle of the bicycle frame can alter the x-axis alignment of the bicycle frame body with the ramp, making direct x-axis optimization unreliable.

The goal is defined as:

$$J_{\text{final\_output}} = w \cdot (o(t_f))^2 \tag{3.4}$$

Where:

- $J_{\text{final\_output}}$ is the cost associated with minimizing or constraining the final output.
- w is the weight assigned to the goal.
- t_f denotes the final time of the trajectory.
- $o(t_f)$ is the output at the final time. In this case, the magnitude of the bicycle frame position.

The weight assigned to this goal is -0.2.

Optimizing Linear Bicycle Velocity

To optimize the linear bicycle velocity, the `MocoOutputGoal` is used. The objective function for the `MocoOutputGoal` integrates a model output $o(t)$ over time is given by:

$$J_{\text{output}} = \int_{t_i}^{t_f} w \cdot o(t)\, dt \tag{3.5}$$

Where:

- J_{output} is the cost associated with minimizing or constraining the output.
- w is the weight assigned to the goal.
- $o(t)$ is the output value at time t.
- t_i is the initial time.
- t_f is the final time.

It is used to maximize the magnitude of the linear bicycle frame velocity at the rear hub of the bicycle.

The weight assigned to this goal is -0.8.

Minimizing the Bicycle Pitch Angle

The *MocoStateTrackingGoal* is used to minimize the pitch angle of the bicycle. It aims to minimize the difference between the simulated state variables and a set of reference state variables over a given phase. In this case, it is used to penalize excessive pitch angles of the bicycle frame, guiding the solution towards maintaining a pitch angle close to zero. However, it allows for deviations when it is significantly more favourable, such as when lifting the front wheel to pass the gate.

The goal can be expressed mathematically as:

$$J_{\text{state\_tracking}} = \int_{t_0}^{t_f} \sum_i w_i \left(x_i(t) - r_i(t)\right)^2 \, dt \tag{3.6}$$

Where:

- $J_{\text{state\_tracking}}$ is the cost associated with state tracking.
- t_0 and t_f are the initial and final times of the phase, respectively.
- w_i is the weight assigned to state variable i.
- $x_i(t)$ is the value of state variable i at time t.
- $r_i(t)$ is the reference value for state variable i at time t.

The weight assigned to this goal is 3.

Minimize Control Effort

To minimize control effort, the *MocoControlGoal* is used. It is designed to minimize the integrated sum of the absolute values of the control signals, each raised to a specified exponent, over the entire phase (Equation 3.7). It aims to minimize control efforts throughout the movement. This cost term is particularly useful in cases where multiple solutions are possible, as it selects the solution with the least control effort as the optimal one.

It is calculated with the following equation:

$$J_{\text{control}} = \frac{1}{d} \int_{t_i}^{t_f} \sum_{c \in C} w_c \left|x_c(t)\right|^p \, dt \tag{3.7}$$

where:

- J_{control} is the cost associated with minimizing the controls.
- d represents the displacement of the system if `divide_by_displacement` is true; otherwise, d is set to 1 when `divide_by_displacement` is false.
- t_i is the initial time.
- t_f is the final time.
- C is the set of control signals.
- w_c is the weight assigned to a control signal c.

- $x_c(t)$ is the value of control signal c at time t.
- p is the exponent.

Divide by displacement is set to true, w_c is set to one for all controls and p is kept as the default of two, to make the cost function the sum of squares to minimize the control effort for the BMX gate start. The weight assigned to this goal is 0.01.

3.2.2. Optimization Solver

To solve the optimal control problem, the *MocoSolver* employs the CasADi library [43] to transform the continuous optimal control problem defined by the *MocoProblem* into a finite-dimensional nonlinear program (NLP). This process involves transcription, where the continuous problem is discretized into a form that can be handled by numerical solvers.

The transcription of the continuous-time optimal control problem into a discrete-time problem in the BMX optimization is achieved using the Hermite-Simpson transcription scheme as explained in Chapter 2. This method is preferred for problems requiring high precision and stable solutions, such as the BMX start optimization. Additionally, the BMX start model includes non-linear components, such as contact forces, which necessitate the use of an advanced transcription method like Hermite-Simpson instead of the Trapezoid transcription scheme.

In the optimal control problem of the BMX start, the convergence tolerance was initially set to 10^{-2}, the constraint tolerance to 10^{-3}, and the number of mesh intervals to 70, equating to 0.0189 s per step to allow for faster convergence. These parameters were gradually adjusted to improve the accuracy of the solution. The number of mesh intervals was increased to 250 (0.0053 s per step) to provide a finer resolution of the trajectory, and the convergence tolerance was tightened to 10^{-5} to ensure a more precise optimization outcome in the simulations with the 'Upper Body Model', and tightened to 10^{-3} in the simulations with the 'Full Body Model'. These adjustments help balance computational efficiency with the accuracy of the results.

Initial Guess

An initial guess can be provided in the *MocoSolver* class.

A crucial aspect of solving the optimal control problem is establishing a robust initial guess to prevent entrapment in local minima, particularly due to the non-linear nature of the dynamics involved and to increase the decrease the computational time.

To accomplish the first goal of the thesis: Optimizing the whole BMX start, including the recoil, using optimal control. The BMX start is segmented into two phases to manage complexity:

1. **Recoil Phase**: The bicycle rolls backward to the maximum extent possible within a designated timeframe.
2. **Forward Phase**: The bicycle accelerates forward, aiming to achieve the greatest linear velocity.

For each phase, the state variables are constrained within joint limits (Table 3.1.2), and control values for actuators range between -1 and 1, except for the crank torque, which is restricted from 0 to 1 due to the free-hub mechanism on the BMX's rear wheel.

The results of the optimal control problem, solved separately for the recoil and forward phases, are combined and used as an initial guess for the optimization of the entire movement. They could be integrated because the final time and positions of the recoil phase are used as the initial conditions for the forward phase. The recoil and forward phases influence each other, so the separate results are not suitable as final results. However, they provide a valuable initial guess. Without this initial guess, the optimal control problem often failed to converge to an optimal solution. Even when it did, the bicycle did not exhibit backward movement, and the final velocity was lower, indicating that the solution was trapped in a local minimum.

Recoil

Firstly, the recoil movement is solved. The initial bounds for the positions of all joints are the default values of the joints, which are the initial angles and positions from the experimental data. The initial horizontal bicycle frame position and pitch angle are bounded to zero. The initial velocity is zero for all

joints, with the final horizontal bicycle velocity also bounded to zero. This ensures that at the end of the recoil phase, the bicycle is stationary, ready to transition into the forward phase.

The objective function consists of a *MocoControlGoal* and a *MocoFinalOutputGoal*. The *MocoFinalOutputGoal* targets the magnitude of the bicycle frame's position, with a weight of 0.1. This objective aims to minimize the horizontal bicycle's position, seeking a solution where the bicycle moves as far backward as possible within the time frame of 0.18 to 0.3 s, corresponding to the typical duration of the recoil phase observed in video footage.

Forward
The second part is the 'forward' phase where the bicycle should reach the highest linear velocity in the direction. This phase lasts from 0.3 s until 0.67s, when the gate is completely open (Figure 1.1.2). The initial positions are bounded to the final position of the solution of the recoil optimization, and the initial velocities are set to zero. The objective function for this phase includes a *MocoControlGoal* and a *MocoOutputGoal*, with the latter focusing on maximizing the magnitude of the bicycle frame's linear velocity, weighted at -0.2.

Whole BMX Start
The solutions from the recoil and forward phases are combined into one *MocoTrajectory* to be used as an initial guess for the optimization of the entire BMX start. This step is crucial because, without a robust initial guess, the optimal control problem for the whole BMX start fails to converge to an optimal solution.

Upon retrieving the first solution for the entire movement, the model and optimal control problems were incrementally made more complex. Subsequent successful results were then used as new initial guesses. This involved adding activation dynamics to the ideal actuators, incorporating a cost term for the bicycle's pitch angle, reducing the damping, and replacing the *CoordinateLimitForce* with contact forces between the gate and the front wheel, and between the front wheel and a platform.

The nominal objective function for the entire movement comprises a *MocoOutputGoal* to maximize the linear bicycle velocity with a weight of -0.8, a *MocoFinalOutputGoal* to maximize the final bicycle position with a weight of -0.2, a *MocoStateTrackingGoal* to penalize large pitch angles of the bicycle with a weight of 3, and a *MocoControlGoal* to slightly minimize the control effort with a weight of 0.01. The optimization process for the whole movement spans up to 1.5 s.

3.2.3. Model Validation Using an Optimal Tracking Simulation

An optimal control problem formulated as an optimal tracking problem was solved using a *MocoStateTrackingGoal* (Equation 3.6) to validate the 'Full Body Model'. The objective of such an optimal tracking problem is to find the best set of controls that minimize the difference between the given states and the simulation results.

The cost function consisted of a *MocoStateTrackingGoal* with a weight of 5, a cost term for minimizing the pitch angle of the bicycle with a weight of 3, and the MocoControlGoal with a weight of 0.01.

The specific weights applied to the joints in the *MocoStateTrackingGoal* were as follows:

- The hips, knees, ankles, shoulder, elbow, and hand flexion angles had a weight of 1.
- The crank angle had a weight of 3.
- The rear wheel rotation, front wheel rotation, bicycle frame pitch angle and bicycle frame horizontal translation had a weight of zero.

These weights ensured that the model accurately tracked the desired angles during the validation task, with an emphasis on tracking the crank angle to obtain a good representation of the crank torque.

The RMSE between the experimental joint angles and simulated joint angles will be calculated to evaluate if the model accurately reproduces experimental data, indicating its validity. Additionally, the RMSE between the experimental crank torque and power, along with the Spearman correlation (used due to the non-normal distribution of the data), will be analysed.

Experimental Data

Dilgt [44] from Vrije Universiteit Amsterdam collected kinematic data using five elite BMX SX athletes to calculate mechanical power output based solely on kinematics. An Xsens MVN suit (Xsens Technologies, Enschede, The Netherlands) with high-frequency IMU sensors captured the movement of the rider and the rotation of the rear hub. The Xsens software uses sensor fusion techniques to combine data from accelerometers, gyroscopes, and magnetometers, resulting in segment rotations and translations.

To align the data with the bicycle rider model, which only allows planar rotations, the 3D joint angles from the Xsens system needed conversion. This was done using OpenSense[10], part of OpenSim, which converts experimental IMU data into OpenSim generalized coordinates. OpenSense projects the measured data onto the OpenSim model, finding the best solution matching the constraints without needing to scale the model to the specific participant.

OpenSense processed the IMU data of six lower limb sensors, the pelvis, and the rear wheel, resulting in nine joint angles, the crank angle, and the rear wheel angle, without accounting for forces or providing angular speeds and joint torques.

The data processing was done by Groenhuis [6]. The position and rotation of the L5 joint in the local coordinate system of the bicycle frame were calculated for the horizontal torso position and lean angle. The kinematics of the second trial of one female Dutch Elite rider were used in this thesis.

Grieken [33] from Delft University of Technology collected kinetic data from the same participants but on different days and bicycles using a fully instrumented bicycle. This setup included a Swift Axis2D crank, which measures the pedal forces in both radial and tangential directions at a frequency of 100 Hz, as well as crank rotation and velocity. The data, gathered during six all-out starts from a BMX SX ramp, was used to validate the optimal tracking results.

3.3. Simulations for Different Research Goals

Goal 1: Optimal control simulation of the whole BMX start, including the recoil phase.
This was achieved by using the 'Upper Body Model' and solving the optimal control problem for the recoil and forward phases separately. Then we used these combined solutions to solve the whole movement, with the nominal objective function of: maximizing the magnitude of the linear velocity of the bicycle frame, maximizing the final position of the bicycle frame, minimizing the bicycle frame pitch angle, and slightly minimizing control effort.

Goal 2: Influence of rider strength. We changed the maximal crank torque to investigate the influence of rider strength on the kinematics by solving the optimal control problem for a range of maximal crank torques (250 Nm, 275 Nm, 300 Nm, 325 Nm, and 350 Nm). The 'Upper Body Model' was used with the nominal cost function.

Goal 3: Influence of Reaction Time. We investigated the influence of reaction time on start performance by solving the optimal control problem for a range of reaction times (0.14 s, 0.16 s, and 0.18 s after the red light) using the nominal cost function with the 'Upper Body Model'.

To study the importance of using the optimal strategy corresponding to the actual reaction time, we investigated whether it would be better to use a 'conservative' start technique for a slower, but more robust reaction time (e.g., 0.18 s) instead of applying the optimal strategies for reaction times of 0.14 s or 0.16 s initiated later at 0.18 s. To do this, we shifted the optimal controls and corresponding states in time, so that the optimal control solutions for reaction times of 0.14 s and 0.16 s started at 0.18 s (a shift of 0.04 s and 0.02 s, respectively).

Goal 4: Validate and verify the 'Full Body Model'. We implemented and verified the 'Full Body Model', which has a better biomechanical representation of the BMX rider. The validation was conducted by solving an optimal tracking simulation (*MocoStateTrackingGoal*), with the objective of finding the control inputs that result in the closest match to the experimentally measured kinematics. Lastly, a predictive optimal control problem was solved with the 'Full Body Model' to get a better biomechanical represen-

[10] https://simtk.org/projects/opensense

tation of the optimal BMX start. Specifically, to better reproduce the torque at the cranks by accurately representing the rider's biomechanics.

4

Results

In this chapter, the results of the optimal control simulations are presented for both the 'Upper Body Model' and the 'Full Body Model'. For the 'Upper Body Model', simulations were conducted under varying crank torques and different reaction times. For the 'Full Body Model', simulations were performed to validate the model and to gain insight into the optimal kinematics and dynamics.

In all optimizations, the primary objective was to maximize the magnitude of the linear velocity of the bicycle, and the final position of the bicycle. Additionally, the controls were slightly minimized, and the pitch angle of the bicycle was minimized to ensure realistic results. To validate the 'Full Body Model', the optimal control problem was cast as an optimal tracking problem.

4.1. Simplified Upper Body Model

The 'Upper Body Model' investigates the influence of maximal crank torque and reaction time on BMX start performance using optimal control methods. Various torque levels (250 Nm, 275 Nm, 300 Nm, 325 Nm, and 350 Nm) and reaction times (0.14 s, 0.16 s, and 0.18 s) were analysed to determine their impact on the kinematic and dynamic behaviours of the BMX rider and bicycle. The results are presented through multiple figures illustrating positions, velocities, controls, and joint forces and torques over the start period from 0.14-0.18 s to 1.2 s. The time taken to reach the kink at 3.15 m is often used as a performance criterion.

First, we solved the optimal control problem for the recoil and forward phases separately to obtain a robust initial guess for the entire BMX start. The joint angles from this initial guess are shown in Figure A.1.1, and the joint forces and torques are detailed in Figure A.1.2 in Appendix A.

4.1.1. The Effect of Maximal Crank Torque on Optimal Start Coordination and Performance

The results for the optimizations with different maximal crank torques (250 Nm, 275 Nm, 300 Nm, 325 Nm and 350 Nm) are displayed.

The left side of Figure 4.1.1 shows the displacement, and the right side shows the velocity of the bicycle frame along the platform. Higher torque levels result in greater displacement after 1.2 s.

For all torque levels, the gate area (from 0.0 m to 0.5 m) is fully crossed by the frame at the same time, coinciding with the time when the gate is fully opened at 0.67 s. The horizontal position remains comparable until the entire bicycle, with a length of 1.62 m, has crossed the pivot point of the gate.

The velocity remains similar from the initiation of the gate drop until the gate is halfway open across all simulations with different maximal crank torques.

Once the gate is fully crossed, the higher crank torque simulations diverge from the lower crank torque simulations, showing increased displacement and velocity for higher crank torques.

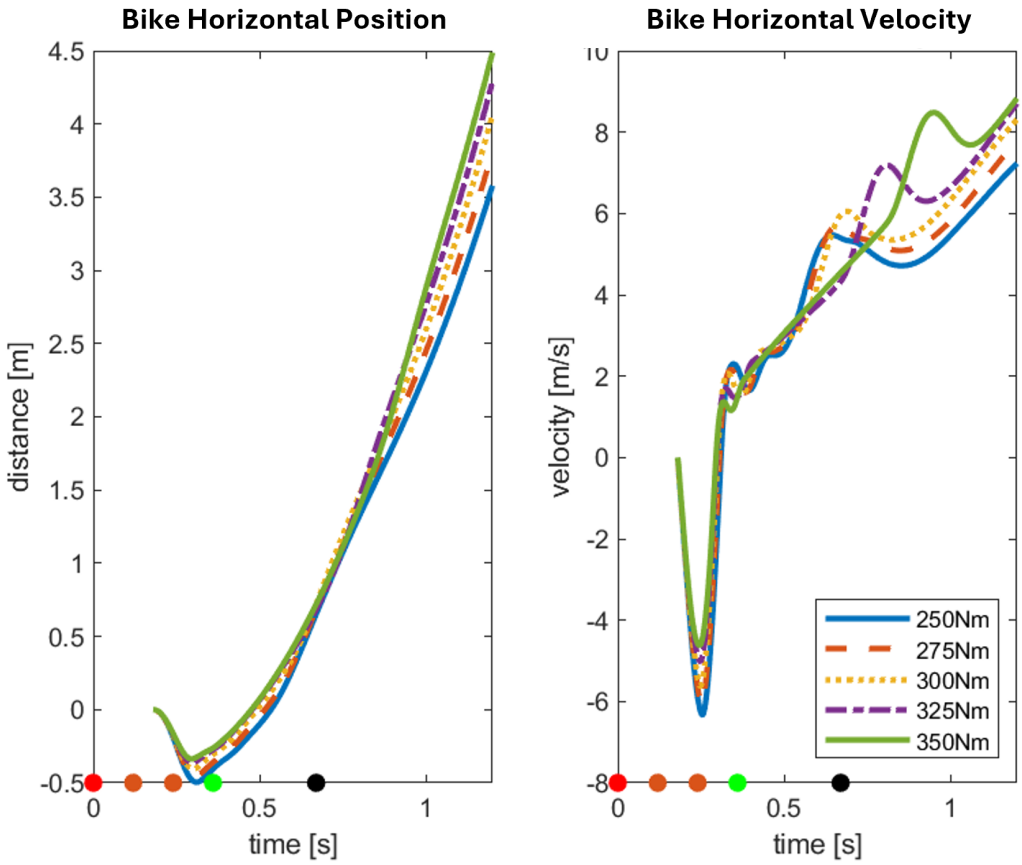

Figure 4.1.1: Linear Horizontal Bicycle Position and Velocity for Different Maximal Crank Torques (250 Nm, 275 Nm, 300 Nm, 325 Nm, and 350 Nm). The figure shows how different levels of crank torque affect the bicycle's position and velocity along the start platform.

Table 4.3.1 presents the time to reach the kink for the various maximal torque levels. The optimal coordination for a lower maximal crank torque is characterized by a greater recoil compared to the highest maximal crank torque of 350 Nm, 0.5 m and 0.34 m respectively (Table 4.3.1 and Figure 4.1.1).

In Figure 4.1.2 the positions and angles of the BMX rider's upper extremities joints are displayed for five different maximal crank torques.

It can be observed that the initial torso forward lean angle decreases for higher maximal crank torques. The forward horizontal torso position is greater for higher maximal crank torques. Conversely, the shoulder flexion angle is greater for lower maximal crank torques (Table A.1.1). These differences result in an initial position with a more backward centre of mass for lower maximal crank torques (Figure 4.1.2b), compared to higher maximal crank torques (Figure 4.1.2c), allowing for a greater recoil. The exact initial positions of all joints can be found in Table A.1.1 in Appendix A.

At the beginning of the movement, the torso flexes and moves forward, the shoulder extends, and the elbow flexes. Approximately when the gate is fully open (0.67s), the torso slides backward, the torso extends, the shoulder flexes, and the elbow flexes.

For the final position, the torso horizontal translation position and the elbow flexion angles are greater for a higher maximal crank torque. While the torso forward lean angle and shoulder flexion angle are smaller for higher maximal crank torques (Figure 4.1.2). This results in a more forward and slightly backward final position of the torso for higher maximal crank torques. This is influenced by the cost term that minimizes the bicycle's pitch angle. The exact final positions of all joints can be found in Table A.1.1 in Appendix A.

In Figure 4.1.3, wheel clearance is displayed for the maximal crank torque of 300 Nm. This is the

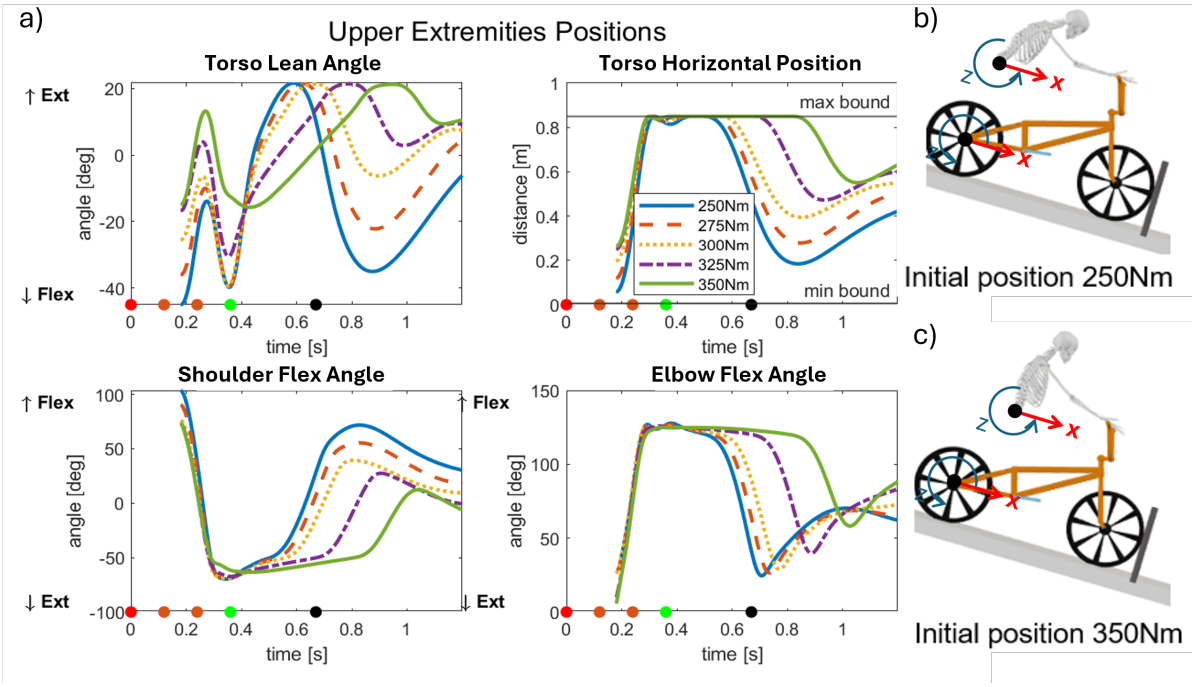

Figure 4.1.2: Position of all Upper Extremities Joints of BMX Rider for Different Maximal Crank Torques (250 Nm, 275 Nm, 300 Nm, 325 Nm, and 350 Nm). This figure illustrates the changes in joint positions of the rider's upper extremities in response to different crank torques. The dots indicate the timing of the start lights: red light at 0 s, first orange light at 0.12 s, second orange light at 0.24 s, and green light at 0.36 s. The gate starts to open at the green light and is fully open at the black dot at 0.67 s.

distance between the start platform and the bottom of the wheel.

Joint Actuators

The torques and forces from the actuators for the simulations with different maximal crank torques are displayed in Figure 4.1.4. The activation dynamics smooth the control signals over time. The plots illustrate the forces and torques applied to the joints of the rider and bicycle. The activation patterns vary with different maximal crank torques. A detailed figure, with the control data, can be found in Figure A.1.3 in Appendix A.

Torso Force/Torques: Figure 4.1.4 shows the force applied in the torso's translational direction. At the start, the force is maximized to move the torso forward, then it rapidly becomes maximally negative to decelerate. This pattern aligns with the initial phase of the movement, where the centre of mass (CoM) is first moved forward to propel the bicycle backward. When the gate starts opening (at 0.36 s), the forces begin to oscillate and then stabilize over time. A similar pattern is observed for the acting around the torso lean angle. Initially, the positive torque flexes the torso forward, followed by a negative torque that extends the torso, and then it flexes again after 0.7 s.

Crank Torque: The crank torque is maximally activated in all simulations from the start to the end of the movement.

Shoulder Flexion Torque: The torque applied at the shoulder joint is initially maximally negative to extend the shoulder, then it becomes maximally positive to flex the shoulder. After the gate starts to open, the shoulder torque stabilizes and approaches approximately -60 Nm.

Elbow Flexion Torque: The torque applied to the elbow joint initially starts at approximately -50 Nm and then quickly increases to near the maximum positive value, to flex the elbow. Following the gate opening, the torque around the elbow stabilizes and approaches approximately 25 Nm.

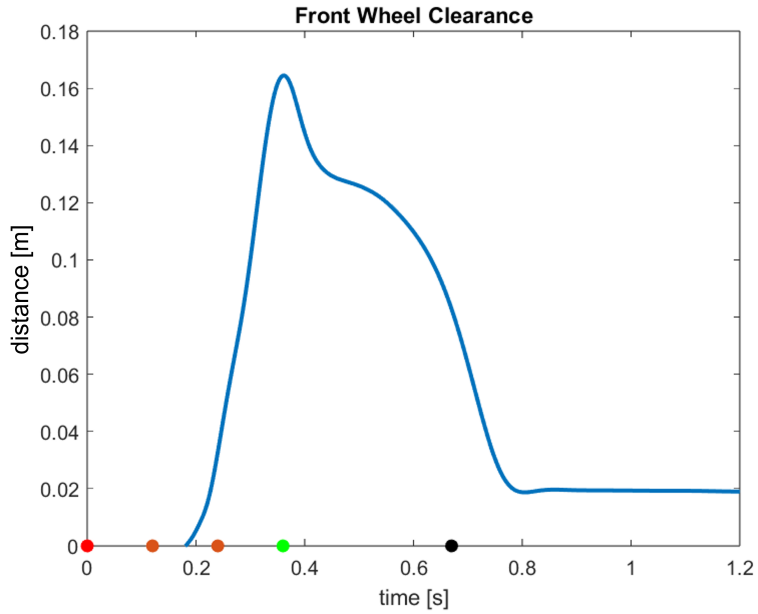

Figure 4.1.3: Distance Between the Bottom of the Front Wheel and the Platform During the Start. This figure shows the vertical distance between the bottom of the front wheel and the surface of the platform during the baseline simulation, with a maximal crank torque of 300 Nm. The dots indicate the illumination of the start lights: red, first orange, second orange, and green. The gate starts opening at the green light and is fully open at the final black dot.

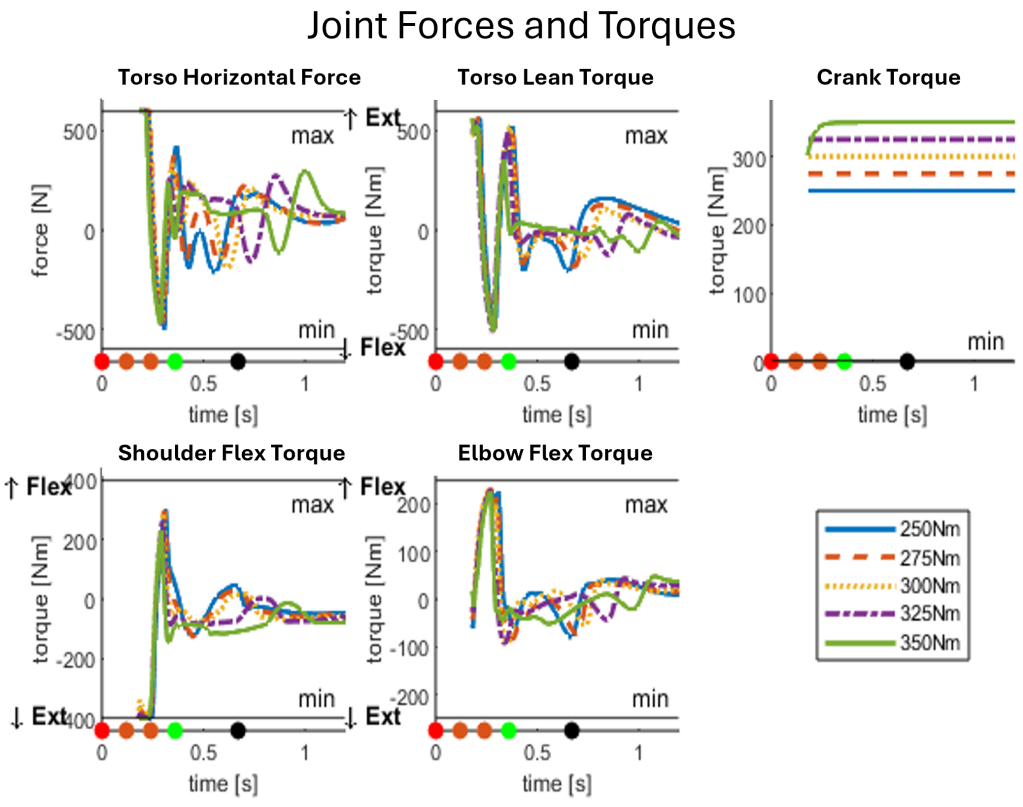

Figure 4.1.4: Joint Forces and Torques for Different Maximal Crank Torques. This graph details the Forces and Torques at various joints for five different maximal crank torques (250 Nm, 275 Nm, 300 Nm, 325 Nm and 350 Nm). The horizontal lines depict the minimal and maximal force/torque of the actuator. The dots indicate the illumination of the start lights: red, first orange, second orange, and green. The gate starts opening at the green light and is fully open at the final black dot.

4.1.2. Different Reaction Times

The predictive optimal control simulations were performed for various reaction times, namely 0.14 s, 0.16 s, and 0.18 s, with a maximal crank torque of 300 Nm. The resulting positions, velocities, and activations showed consistency, with minor phase shifts corresponding to the different reaction times. Figure 4.1.5 shows the position and velocity of the bicycle frame x coordinate for different reaction times. In Figure 4.1.6, the positions of the joints of the upper extremities are displayed, showing the same trajectory with a phase shift corresponding to the reaction time difference. The velocity at the gate drop (0.67 s) is virtually identical for all three reaction times. The forces and torques for all actuators in the 'Upper Body Model' for three different reaction times can be found in Figure A.1.4 in Appendix A.

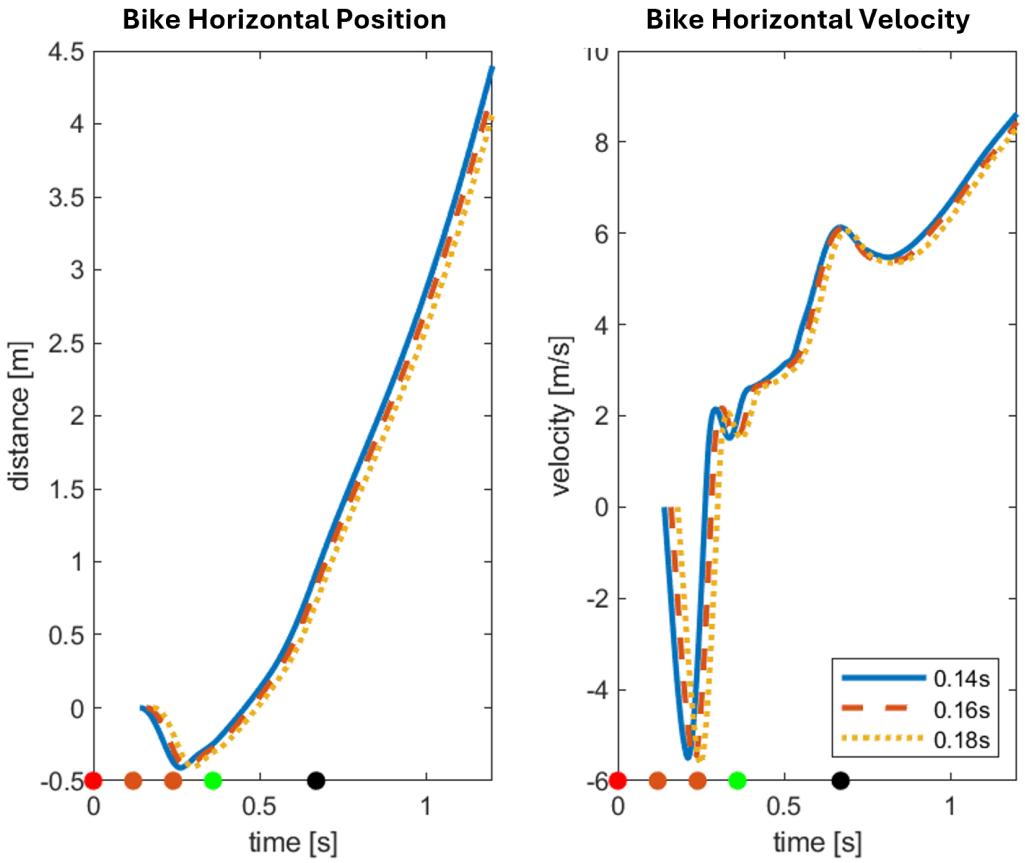

Figure 4.1.5: Linear Horizontal Bicycle Position and Velocity for Different Reaction Times (0.14 s, 0.16 s, 0.18 s). This figure shows how different rider reaction times impact the linear horizontal position and velocity of the bicycle during the start. The figure shows a phase shift which corresponds to the difference in reaction time. The dots indicate the illumination of the start lights: red, first orange, second orange, and green. The gate starts opening at the green light and is fully open at the final black dot.

It was investigated whether it would be better to use a 'conservative' start technique for a slower, but more robust reaction time (e.g., 0.18 s) instead of applying the optimal strategies for reaction times of 0.14 s or 0.16 s initiated later at 0.18 s. To do this, the optimal controls and corresponding states are shifted in time, so that the optimal control solutions for reaction times of 0.14 s and 0.16 s started at 0.18 s (a shift of 0.04 s and 0.02s, respectively). Since all optimal techniques for all starting times were identical, this did not make a difference in the achieved performance (Figure A.1.4).

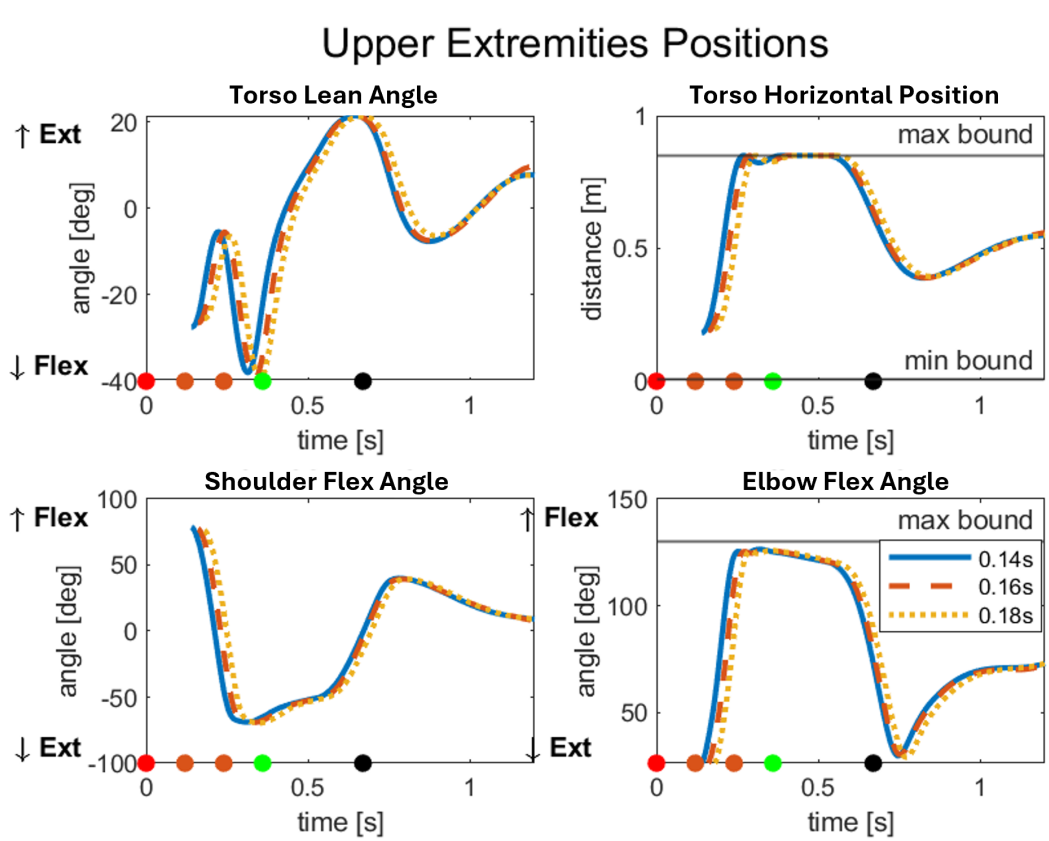

Figure 4.1.6: Positions of All Joints of the 'Upper Body Model' for Different Reaction Times (0.14 s, 0.16 s, 0.18 s). The figure shows a phase shift which corresponds to the difference in reaction time. The dots indicate the illumination of the start lights: red, first orange, second orange, and green. The gate starts opening at the green light and is fully open at the final black dot.

4.2. Full Body Model

We conducted two simulations using the 'Full Body Model'. First, an optimal tracking simulation to validate our model against experimentally measured data, and second, a predictive simulation aimed at maximizing start performance.

4.2.1. Optimal Tracking Simulation for Validation

An optimal tracking simulation was performed to validate the 'Full Body Model' against experimental data. The RMSE values between the experimental joint angles and the results of the optimal tracking optimization are listed in Table 4.2.1.

The mean RMSE across all joints for the entire movement (between 0.187 and 1.2 s) was 2.18°° with the upper extremities averaging 2.03° and the lower extremities averaging 2.24°.

The mean RMSE was higher during the recoil phase, at 3.30°, compared to 1.83° during the forward phase. For the RMSE of the optimal tracking during the recoil phase, the time period from 0.187s (the start of the experimental data and movement) to 0.38s was considered. The recoil actually lasts until 0.37 s 4.3.1), but 0.38s was chosen to match the start of the optimal tracking simulation in the study by Groenhuis [6], allowing for better comparison.

The RMSE between the experimental data collected by Grieken [33] for three trials, and the optimal tracking and predictive simulations for net crank torque and net crank power, are shown in Table 4.2.3. The crank torque was calculated by multiplying the tangential pedal forces by the crank arm length of 175 mm.

The RMSE $\pm$ standard deviation (SD) between the experimental crank torque data and the optimal tracking simulation was 61.85Nm $\pm$ 4.97 Nm and 59.66 Nm $\pm$ 2.63 Nm for the predictive simulation. The RMSE for the forward phase was lower (60.97 $\pm$ 6.16 Nm) compared to the recoil phase (65.17 $\pm$ 0.59 Nm). The predictive simulation results showed similar values for the whole start (59.66 $\pm$ 2.63 Nm), recoil (56.84 $\pm$ 9.66 Nm) and forward phase (60.11 $\pm$ 5.14 Nm).

The net crank power, calculated by multiplying the net crank torque with the angular velocity of the crank, showed an RMSE of 430.46 W $\pm$ 30.51 W for the whole start in the optimal tracking solution and 559.69 $\pm$ 28.03 W for the predictive simulation.

Coordinate	RMSE Start (deg)	RMSE Recoil (deg)	RMSE Forward (deg)
Right Hip Flexion Angle	2.53	3.96	2.03
Right Knee Flexion Angle	2.31	3.43	1.94
Right Ankle Flexion Angle	1.79	1.77	1.79
Left Hip Flexion Angle	2.57	4.59	1.72
Left Knee Flexion Angle	1.91	2.56	1.71
Left Ankle Flexion Angle	2.30	2.50	2.25
Left Crank Angle	2.33	2.82	2.19
Shoulder Flexion Angle	1.75	3.47	0.91
Elbow Flexion Angle	1.81	3.22	1.22
Hands Flexion Angle	2.54	2.72	2.50
Mean Upper Extremities	2.03	3.14	1.54
Mean Lower Extremities	2.24	3.14	1.91
Mean	2.18	3.30	1.83

Table 4.2.1: Root Mean Square Error (RMSE) Between the Tracked Experimental Joint Angles and the Results of the Optimal Tracking Optimization. The RMSE values are shown for three phases: the whole start (0.19 s to 1.2 s), the recoil phase (0.19 s to 0.39 s), and the forward phase (0.39 s to 1.2 s).

	Start	Recoil	Forward
	Torque Correlation		
Tracking	0.73 ± 0.02	0.65 ± 0.00	0.71 ± 0.01
Predictive	0.71 ± 0.03	0.80 ± 0.00	0.74 ± 0.02
	Power Correlation		
Tracking	0.89 ± 0.02	0.37 ± 0.06	0.80 ± 0.03
Predictive	0.72 ± 0.04	-0.69 ± 0.02	0.57 ± 0.09

Table 4.2.2: Spearman Correlation for Net Crank Torque and Power. The correlation coefficients (mean ± SD) are calculated between three experimental measurements TU (not tracked) and the results from the optimal tracking and predictive simulations. The correlation values are presented for the entire start (0.19 s to 1.2 s), the recoil phase (0.19 s to 0.39 s), and the forward phase (0.39 s to 1.2 s). Interpretation of correlation strength: very weak (0.00-0.10), weak (0.10-0.30), moderate (0.30-0.50), strong (0.50-0.70), very strong (0.70-1.00).

	Start	Recoil	Forward
	Torque RMSE (Nm)		
Tracking	61.85 ± 4.97	65.17 ± 0.59	60.97 ± 6.16
Predictive	59.66 ± 2.63	56.84 ± 9.66	60.11 ± 5.14
	Power RMSE (W)		
Tracking	430.46 ± 30.51	186.59 ± 25.88	471.47 ± 34.56
Predictive	559.69 ± 28.03	609.87 ± 26.35	546.09 ± 40.07

Table 4.2.3: Root Mean Square Error (RMSE) for Net Crank Torque and Power. The RMSE (mean ± SD) is calculated between three experimental measurements TU (not tracked) and the results from the optimal tracking and predictive simulations. The RMSE values are presented for the entire start (0.19 s to 1.2 s), the recoil phase (0.19 s to 0.39 s), and the forward phase (0.39 s to 1.2 s).

4.2.2. Predictive Optimal Control Results

The predictive optimal control solution for the start with the 'Full Body Model' shows significant improvement compared to the experimental data in terms of kink time, final horizontal bicycle position and final horizontal bicycle velocity (Table 4.3.1). The time to the kink is 1.15 s in the predictive optimal control simulation, compared to 1.23 s in the experimental data. The final frame position is considerably greater (3.64 m compared to 2.93 m), and the final velocity is 8.22 m/s compared to 7.01 m/s in the experimental data. The recoil distance is comparable at 7 cm compared to 8 cm in the experimental data, although the timing differs. The maximal recoil is reached earlier in the predictive simulation (at 0.30 s) compared to the experimental data (at 0.39 s).

There is a small difference in the initial position (Figure 4.2.6a). The lead in the predictive solution is already evident at the gate drop (Figure 4.2.6b), and this lead is gradually extended until the kink (Figure 4.2.6c).

Figure 4.2.1 displays the horizontal bicycle position, the angle of the crank, and the pitch angle of the bicycle. The evolution of the crank angle appears comparable to the experimentally measured crank angle. The bicycle pitch angle increases from zero to 17 degrees within 1.2 s, indicating a significant tilt of the bicycle frame during the start.

Figure 4.2.2 shows the positions of the upper extremities, including the shoulder, elbow, and hand angles. The model indicates considerable movement in the upper body.

Figure 4.2.3 plots the positions of the lower extremities. The hip, knee, and ankle angles demonstrate the pedalling motion, which is essential for the initial acceleration phase.

Figure 4.2.4 illustrates the forces and torques of all *ActivationCoordinateActuators*. These plots show how different joints are engaged throughout the start, providing insight into the coordination required for optimal performance.

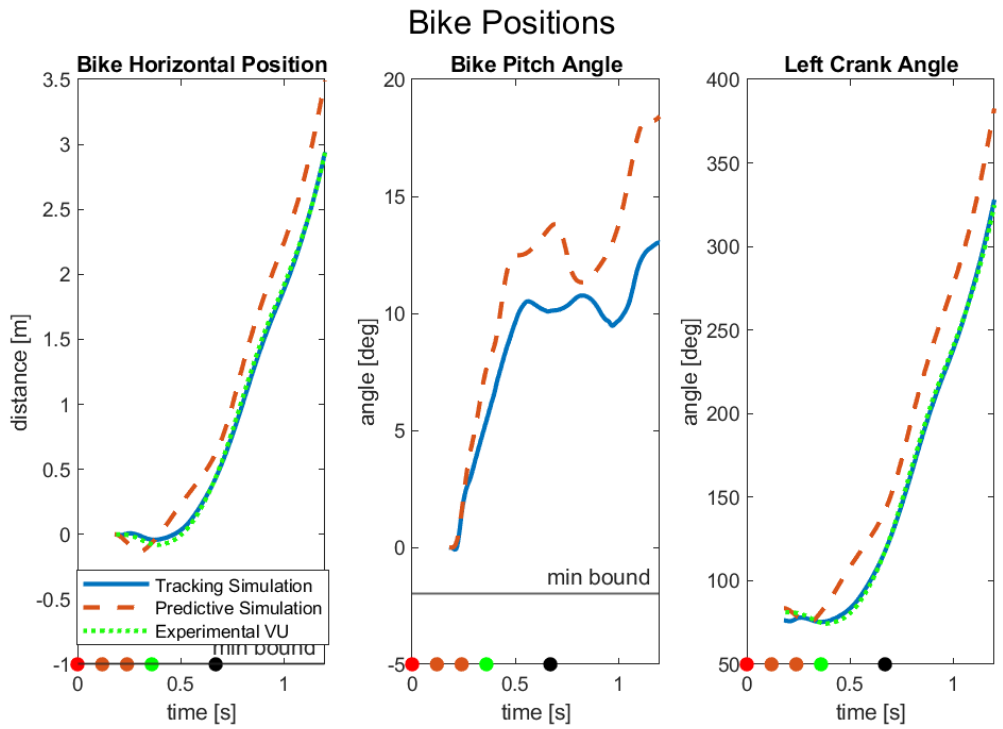

Figure 4.2.1: Linear Bicycle Position, Bicycle Pitch Angle and Left Crank Angle of the 'Full Body Model'. For an optimal tracking and predictive simulation, together with the experimentally collected data by the VU. The horizontal position of experimental data is calculated from the experimental rear wheel rotation. The dots indicate the illumination of the start lights: red, first orange, second orange, and green. The gate starts opening at the green light and is fully open at the final black dot.

During the BMX start simulations, the maximal damping forces in the joints were observed at 0.23 s. The highest damping force recorded in the elbow joint was -67 N, while the shoulder joint experienced a maximal damping force of 71 N. The average damping force across all joints throughout the entire movement was 36 N.

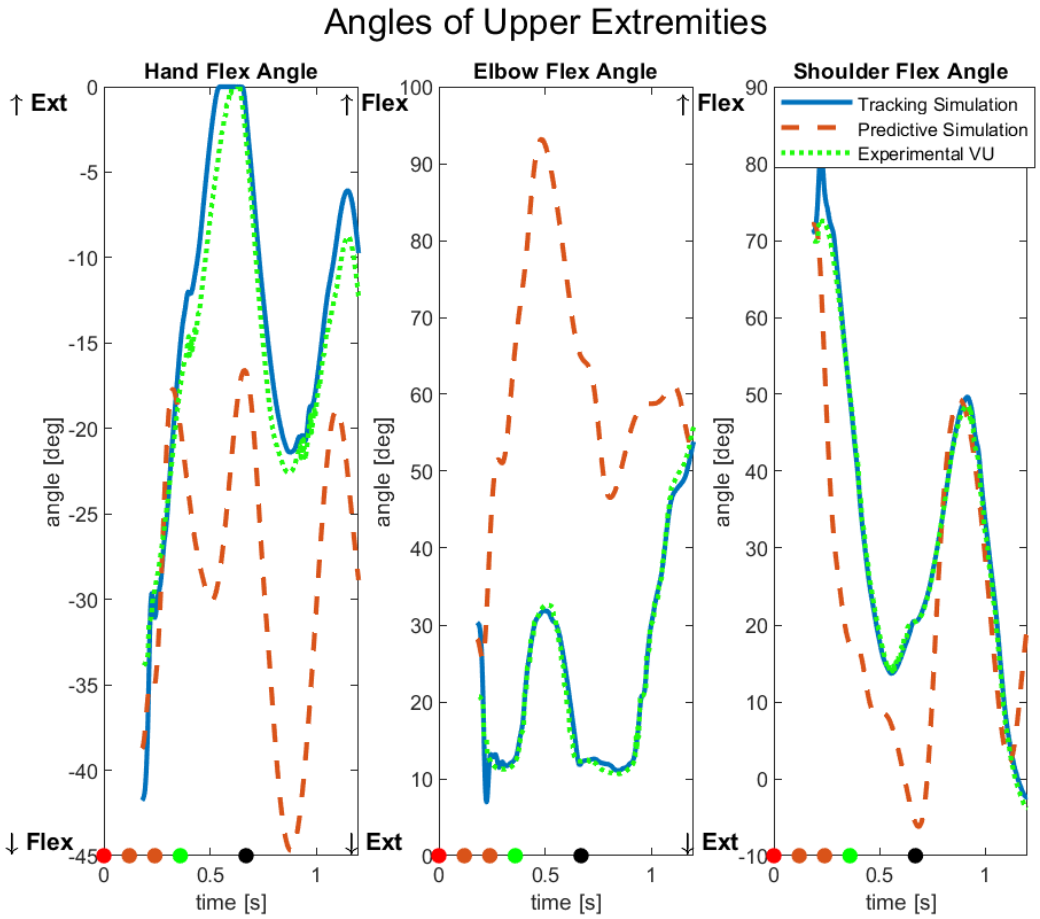

Figure 4.2.2: Angles of Upper Extremities in 'Full Body Model'. Positions of the upper extremities (shoulder, elbow, and hand flexion angles) for a predictive and optimal tracking simulation, along with the experimentally collected data. The dots indicate the illumination of the start lights: red, first orange, second orange, and green. The gate starts opening at the green light and is fully open at the final black dot.

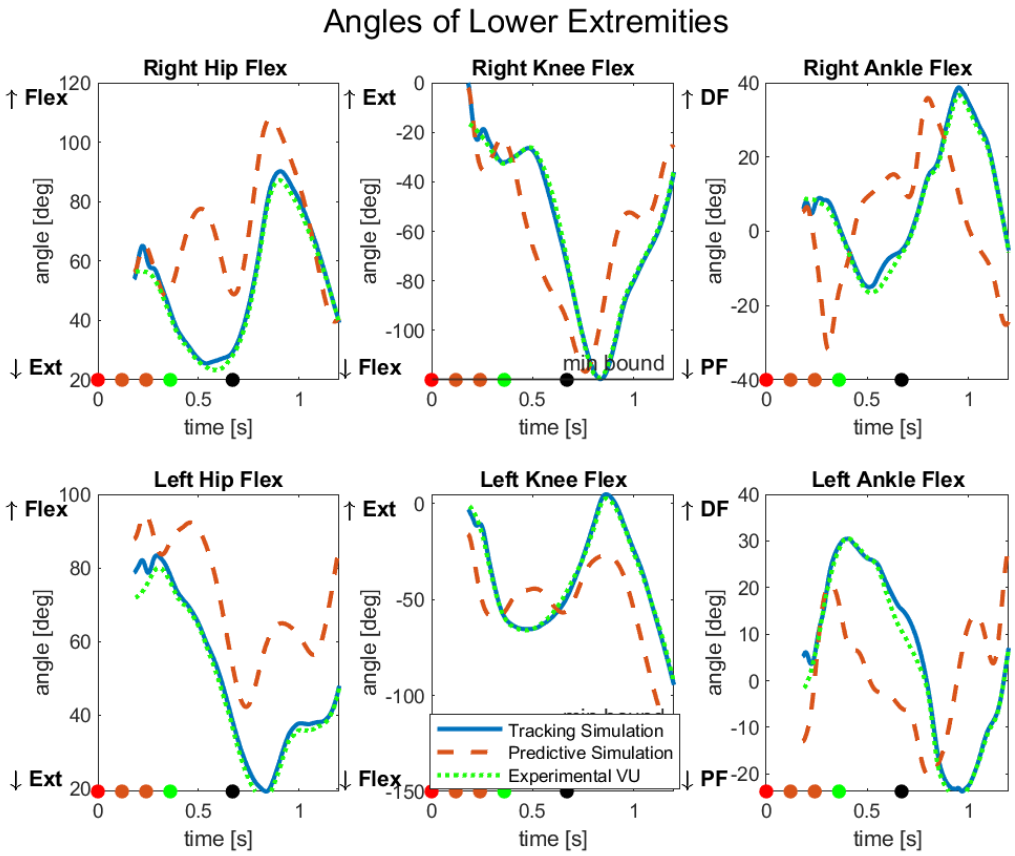

Figure 4.2.3: Angles of Lower Extremities in 'Full Body Model'. This figure shows the positions of the lower extremities (hip, knee, and ankle angles) for a predictive and optimal tracking simulation, together with the experimentally collected data by the VU. The dots indicate the illumination of the start lights: red, first orange, second orange, and green. The gate starts opening at the green light and is fully open at the final black dot.

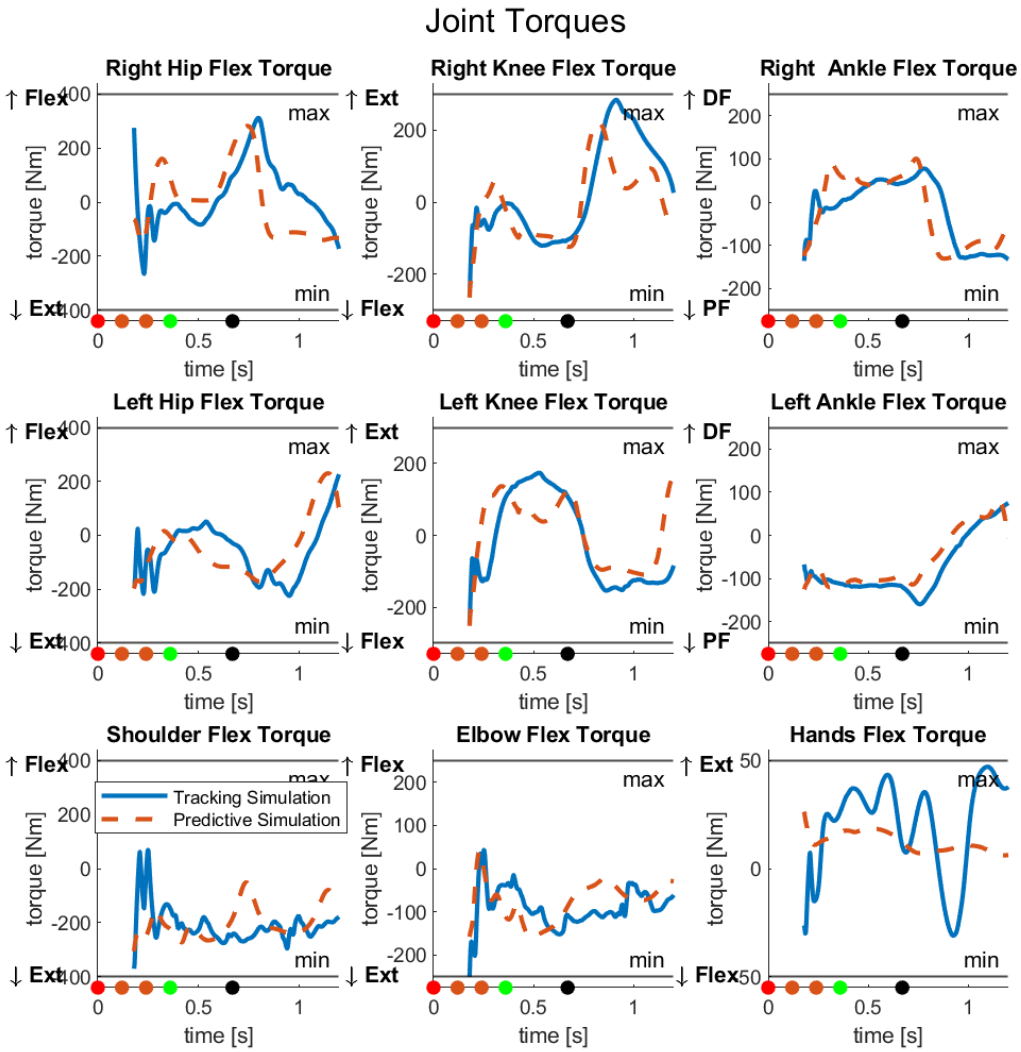

Figure 4.2.4: Joint Torques in 'Full Body Model', for a predictive and optimal tracking simulation. The dots indicate the illumination of the start lights: red, first orange, second orange, and green. The gate starts opening at the green light and is fully open at the final black dot.

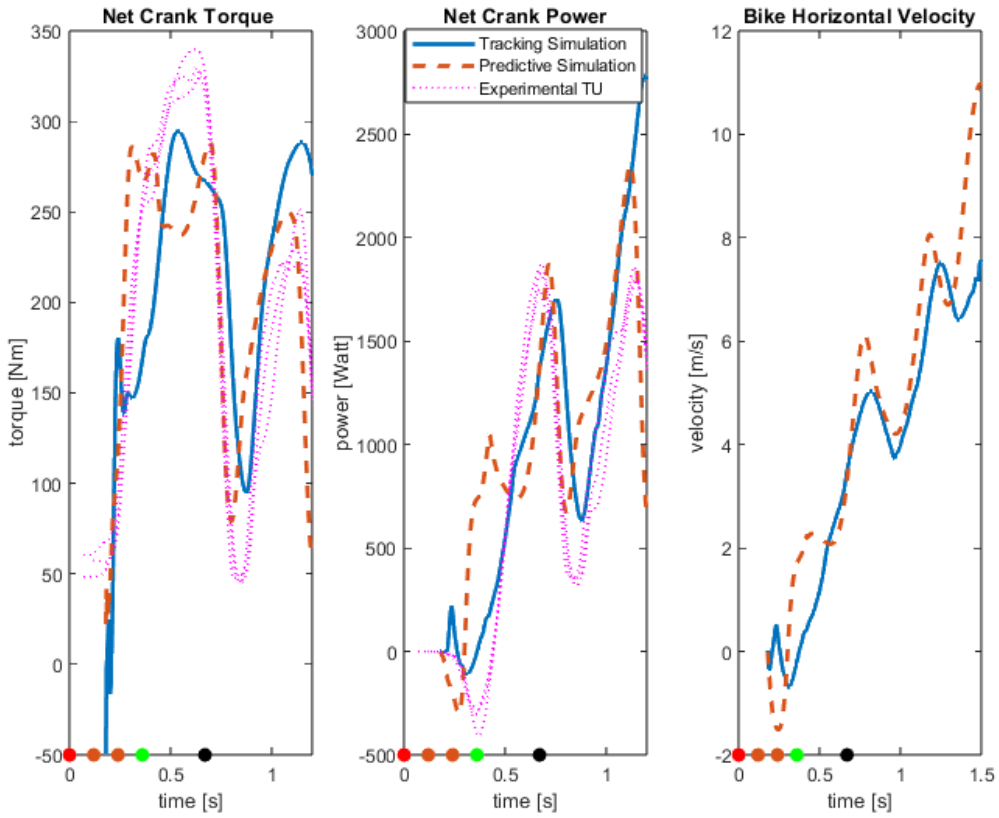

Figure 4.2.5: Net Crank Torque, Power, and Horizontal Bicycle Velocity in 'Full Body Model'. For a predictive and optimal tracking simulation compared with the experimentally net crank torque and power, assessing model performance. The dots indicate the illumination of the start lights: red, first orange, second orange, and green. The gate starts opening at the green light and is fully open at the final black dot.

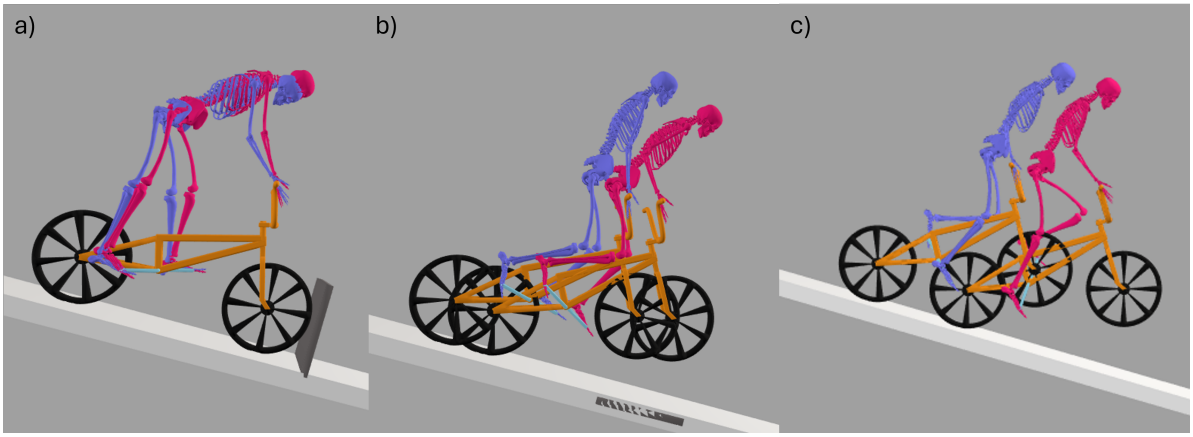

Figure 4.2.6: Initial Position (a), Position at Gate Drop (b), and Final Position at 1.2 s (c). The model in blue is the result of the optimal tracking simulation and in red is the result of the predictive simulation. This figure shows the rider's position at three key stages of the start, comparing tracking and predictive simulation results.

4.3. Performance Metrics

Table 4.3.1 summarizes the key performance metrics for different maximal crank torques and reaction times using the 'Upper Body Model', and tracking and predictive results with the 'Full Body Model', together with the experimental data.

	Time Recoil (s)	Recoil Distance (m)	Velocity Onset Gate Drop (m/s)	Velocity Gate Drop (m/s)	Time to Kink (s)	Kink Velocity (m/s)
250 Nm	0.31	-0.50	2.17	5.39	1.14	6.73
275 Nm	0.31	-0.45	1.86	5.68	1.11	6.92
300 Nm	0.30	-0.41	1.57	5.97	1.08	7.17
325 Nm	0.30	-0.36	1.50	4.34	1.06	7.14
350 Nm	0.30	-0.34	1.55	4.55	1.04	7.76
0.14 s	0.26	-0.41	1.97	6.13	1.04	7.13
0.16 s	0.28	-0.41	1.50	6.10	1.06	7.15
0.18 s	0.30	-0.41	1.57	5.97	1.08	7.17
Tracking	0.37	-0.04	-0.16	3.50	1.23	7.43
Predictive	0.30	-0.13	1.72	3.34	1.16	7.84
Experimental VU*	0.39	-0.08	-0.61	2.22	1.23	5.23

Table 4.3.1: BMX Start Performance Metrics. This table summarizes the key performance metrics for different maximal crank torques and reaction times using the 'Upper Body Model', as well as tracking and predictive results with the 'Full Body Model'. Velocities and distances refer to the horizontal bicycle position or velocity. Metrics include time to recoil, recoil distance, velocity at the onset of gate drop, velocity at gate drop, time to kink, and kink velocity. *Calculated from rear wheel rotation.

5

Discussion

The primary objective of this study was to gain deeper insights into the optimal timing, kinematics, and dynamics of the BMX start, with the ultimate goal of optimizing performance at the start of a BMX race by employing optimal control techniques.

This involved investigating two key scenarios with a simplified torque-driven model: the impact of maximal crank torque on kinematics and the influence of reaction time on kinematics. Additionally, we verified whether a full-body torque driven model could replicate experimental data using an optimal tracking simulation, and we solved a predictive optimal control problem to study what changes to the technique could improve the start performance.

5.1. Key Findings

Goal 1: Adapt the model of Groenhuis [6] to enable simulation of the recoil phase. We simplified the model by Groenhuis [6], to a model with a simplified leg-to-crank actuation.

In this model, the 'Upper Body Model', the rider's upper body was detached from the bicycle, and the legs are replaced by a coordinate actuator at the crankshaft. The fifth lumbar vertebra (L5) is connected to the bicycle with a slider and pin joint with actuators. One advantage of this model is its ability to better reproduce the recoil movement. By bounding the lower limit of the crank torque to zero, the bicycle can only move backward by shifting the centre of mass forward, rather than by applying negative torque at the cranks. This accurately reflects real-life mechanics, where the rotation of the cranks is unidirectionally coupled with the rotation of the rear wheel through a free hub mechanism. Additionally, reducing the number of degrees of freedom (DOF) decreases computational time. However, a disadvantage of this 'Upper Body Model' is that it does not account for the angle-dependent nature of real-life crank torque.

By splitting up the optimal control problem of the whole BMX start into a recoil and forward phase and by solving these phases separately, we could attain a good initial guess and with this initial guess, we could solve the optimal control problem of the whole BMX start.

Goal 2: Investigate the influence of rider strength We investigated the effects of rider strength by varying the maximal crank torque between 250 Nm and 350 Nm. Our findings indicate that maximal crank torque significantly affects the kinematics and performance of the BMX gate start. The linear bicycle velocity between the initiation of the gate drop and the point where the gate is halfway open (0.52 s) is comparable for the simulation result with all different maximal crank torques, approximately matching the linear velocity of the gate at the height of the contact point of the front with the gate (if the front wheel would make contact with the gate) (Figure 4.1.1). This finding suggests that the gate falling speed is the rate limiting factor in the BMX start performance. The horizontal bicycle position is also approximately the same at the gate drop (0.67s).

Thus, technique and timing play a more crucial role than maximal crank torque until the point where the gate is halfway open.

The optimal technique in case of a lower maximal crank torque showed a greater recoil distance compared to the simulation results with higher maximal crank torques.

This could be due to the fact that with a smaller maximal crank torque, the propulsive force is less and more distance is needed to propel the bicycle to match the velocity of the gate drop.

To achieve this greater recoil, the centre of mass is positioned further backward in the initial position in the simulation results with a lower crank torque. This allows for a greater forward movement of the mass centre at the start, which leads to a greater recoil due to the conservation of momentum. The recoil helps to generate the necessary momentum to match the velocity of the dropping gate.

Higher crank torques generate a stronger forward force, allowing the bicycle to accelerate more rapidly. Thus, the rider does not need to gain as large a recoil to bring the bicycle to the same velocity as the dropping gate, resulting in a more upright initial position.

With a higher maximal crank torque, the final position is more forward (Figure 4.1.2). This could be due to the higher moment around the rear wheel, which generates a counter torque on the bicycle around the rear hub, caused by the frictional forces at the rear wheel. This counter torque is greater for a higher maximal crank torque, necessitating the rider to shift the centre of mass forward to prevent the front wheel from lifting too far off the ground.

Goal 3: Investigate the influence of reaction time We investigated the influence of reaction time on BMX start performance. Reaction time impacts performance less significantly than maximal crank torque. Contrary to our hypothesis, the control strategy remains consistent for reaction times between 0.14 s and 0.18 s. This indicates that it is not necessary for BMX riders to adjust their technique for minor variations in reaction time (within the range of 0.14 s to 0.18 s), which is advantageous given the natural variability in human reaction times. However, a faster reaction time does have an influence on performance. A faster reaction time of 0.14 s resulted in a faster kink time (3.70% improvement compared to 0.18 s), and a higher bicycle velocity at the kink. The final bicycle position after 1.2 s was 32 cm greater for a reaction time of 0.14 s compared to 0.18 s. This difference is more than half a wheel, which could enable the lead rider to steer into the optimal line.

Goal 4: Implement and verify a complete torque-driven model to better represent the torque at the crank

Optimal Tracking Simulation We implemented a full-body torque-driven model of the BMX rider and bicycle. We validated the model by simulating an optimal tracking problem. The mean RMSE was 2.18° for the entire start (Table 4.2.1). The low RMSE values indicate a close match between the model and experimental data, confirming the model's accuracy in replicating realistic BMX start movements.

The RMSE for the recoil phase in the 'Full Body Model' is higher compared to the forward phase. This discrepancy can be attributed to the bidirectional coupler between the crank and rear wheel rotation, as opposed to a unidirectional coupler, where only forward pedalling results in bicycle propulsion. The bidirectional coupler allows for negative net torque at the crank, causing the rear wheel to propel the bicycle backward. This occurs during the optimal tracking simulation at the movement initiation, leading to unrealistic negative torques and power outputs at the crank (Figure 4.2.5. Such outputs do not accurately reflect the true dynamics of a BMX start, where backward pedalling is not possible due to the free-hub mechanism. Consequently, this bidirectional coupling introduces inaccuracies in representing the real-life BMX start dynamics. However, in the predictive simulation results, this negative torque at the cranks did not occur.

The mean RMSE for all joints during the forward phase was higher (mean RMSE of 1.83°) compared to the results by Groenhuis [6] (0.800°). However, we were able to attain good tracking results for the entire BMX start until 1.2 s (mean RMSE 2.28°), instead of only the forward phase. Several factors likely contributed to the difference in tracking accuracy during the forward phase. Firstly, the damping in all joints was four times lower in the current study (6.25 N·m/rad·s for the upper extremities, and 2.5 N·m/rad·s for the lower extremities), resulting in less stability and robustness in the joint movements. Lower damping reduces the system's ability to absorb energy and mitigate oscillations, leading to increased variability and potentially higher RMSE values.

Additionally, the arm model used in this study differed from that in Groenhuis [6]. The arm in the current

model was 3 mm longer, and the y-location of the shoulder joint was slightly different. This discrepancy in arm length and shoulder joint position can affect the joint angles obtained during the optimal tracking simulation. Specifically, the inverse kinematics process was carried out with the model by Groenhuis [6].

A longer arm changes the kinematic chain's dynamics, potentially leading to less accurate tracking of the experimentally determined joint angles. Since the inverse kinematics model was calibrated for a different arm length, this mismatch could explain the difference in RMSE for the optimal tracking results

The combined effects of lower damping and changes in arm length likely contributed to the higher RMSE observed in the forward phase of the optimal tracking simulation. The reduced damping made the joints more susceptible to oscillations and instability, while the discrepancy in arm length introduced additional inaccuracies in the kinematic calculations.

For comparison, Haralabidis *et al.* [45] conducted a study where the objective was to track kinematics, net joint moments, and filtered ground reaction forces (GRF) during sprinting using a musculoskeletal model with direct collocation optimal control. They found an average RMSE of less than 1.0° for rotational kinematics and 0.2 cm for translational kinematics. Similarly, Lin and Pandy [46] performed an optimal tracking problem using direct collocation to track kinematics and ground reaction forces, reporting an average RMSE of 0.91° and 0.34 cm for walking and 1.46° and 0.59 cm for running. These studies demonstrate the effectiveness of direct collocation methods in achieving high accuracy in tracking biomechanical data.

It's important to note that for explosive movements, such as the BMX start, a higher RMSE could be expected. This is because explosive motions involve rapid changes in velocity and acceleration, leading to greater variability and complexity in the movement patterns. Consequently, capturing these dynamics accurately could be more challenging. The greater variability in high-speed and high-intensity movements makes precise tracking more difficult compared to slower, more controlled, cyclic activities. This could possibly explain the higher RMSE for the tracking by Lin and Pandy [46] for running compared to walking and the higher RMSE in the tracking for the BMX start compared to running and walking. Furthermore, the existing models are largely based on walking motions, so the parameters might not be well suited for tracking explosive tasks such as running/sprinting or the BMX start.

Predictive Optimization

Lastly, we solved a predictive optimal control problem to provide insights into the optimal kinematics and dynamics of the BMX start. The result showed a significant improvement. The kink time of the predictive simulation was 0.07 s faster. The travelled distance was 57 cm greater after 1.2 s compared to the experimental data. The bicycle velocity at the onset of the gate drop was considerably higher compared to the experimental data. In the experimental data, the bicycle was still moving backward at -0.61 m/s, whereas in the predictive results, the bicycle had a velocity of 1.72 m/s.

The recoil distance was greater (13 cm compared to 8 cm) and reached earlier (at 0.30 s compared to 0.39 s). The duration of the recoil with a reaction time of 0.18 s (also 250 Nm to 350 Nm) was comparable with the 'Upper Body Model', though the recoil was significantly larger with the 'Upper Body Model'.

Overall, we have developed a framework for predictive optimal control simulations for the BMX start. This framework simplifies obtaining new results and making adaptations, providing a valuable tool for future studies to explore various hypotheses and refine the model further.

5.2. Comparison with Literature

The reported time to the kink is shorter in the predictive optimal control simulations compared to experimental studies. The kinematics of the simulation with the maximal crank torque were closest to the optimal tracking simulation results. The time to kink for a maximal crank torque of 250 Nm was 1.14 s, considerably faster compared to the experimental data, which had a time to kink of 1.23 s. This difference can be attributed to the constant, maximally activated crank torque in the simulation, unlike the approximately sinusoidal function dependent on the crank angle observed in real pedalling due to the top and bottom dead centres in the pedal stroke (Figure 4.1.4).

The reported recoils of the predictive simulations with the 'Upper Body Model' are considerably greater than in the literature and compared to the experimental data. Grigg [13] reported a recoil of 11.7 ± 0.49 (mean ± SD) cm, which is smaller than the values found in this study with the 'Upper Body Model', ranging from 34 cm to 50 cm. The result of the predictive simulation with the 'Full Body Model' had a recoil distance of 16 cm, which is more comparable to experimental data and literature.

The trajectory of the front wheel hub in Figure 5.2.1 is consistent for all different maximal crank torques, and the shape of the trajectory is between the hairpin and half circle, defined by Grigg [13].

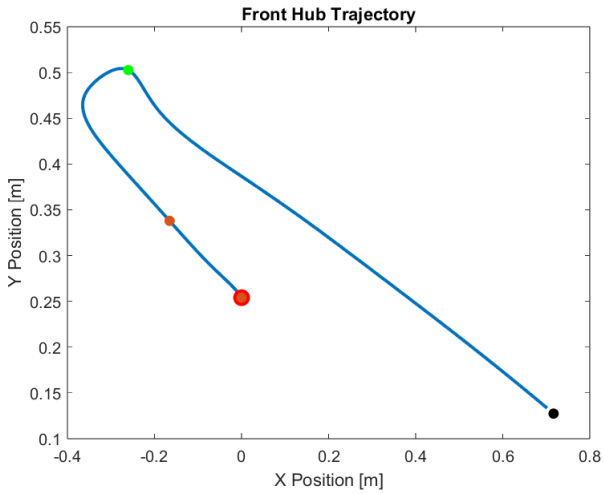

Figure 5.2.1: Simulated Trajectory of Front Wheel Hub. In the global coordinate system between 0 s and 0.67s. From the simulation with the 'Upper Body Model' with a maximal crank torque of 300 Nm.

The wheel clearance between the predictive optimal control solutions and literature is comparable. For all different maximal crank torques, the wheel clearance was maximally 16.5 cm. Grigg [13] reported a mean maximal value during the BMX start of 16.1 $\pm$ 0.04 (mean $\pm$ SD) cm.

5.3. Practical Applications

Our findings suggest that BMX coaches and riders should focus on the technique, timing, and recoil distance of the BMX start. The distance of the recoil is often correlated with the kink time, i.e., a greater recoil correlates with faster kink times Grigg [13]. However, in this research, the recoil distance is not maximized, but it is still significantly greater than the experimentally measured recoils, so optimizing the recoil distance in real life could potentially lead to faster kink times. Additionally, reaction time training could help athletes improve their response to the gate drop, potentially shaving valuable milliseconds off their start times. There is no need to adapt the start strategy for a faster or slower reaction time, since the activations around the joints are exactly the same (for a reaction time between 0.14 s and 0.18 s). Riders with a lower maximal crank torque should start with their body weight positioned further backward to move the bicycle more backward compared to stronger riders. This positioning helps create enough distance to match the velocity of the bicycle to the velocity of the gate.

5.4. Limitations and Future Research

One limitation of this study is the use of the simplified 'Upper Body Model', is the simplified leg-to-crank actuation. While this allowed for the analysis of the effects of net crank torque, the movement of the centre of mass, the movement of the upper body, and the bicycle, it does not capture the angle dependency of the maximal crank torque and the complex biomechanics of a real rider.

The maximal crank torque was modelled as a constant value. This approach is not realistic, as the maximal net crank torque is dependent on the crank angle due to the top and bottom dead centres. The maximal crank torque should vary as a function of time to better reflect actual pedalling dynamics. Moreover, the inertia of the torso was not adjusted to the higher mass of 61.18 kg in the 'Upper Body Model' compared to 20.24 kg for the 'Full Body Model'. The mass was increased to ensure that the

total mass of the rider plus bicycle remained the same in both models. However, with the replacement of the legs with three coordinate actuators for the translational coordinate of the torso in line with the bicycle, the torso lean angle and the crank angle, the mass distribution became less clear. A better approximation of the inertia can certainly be made to improve model accuracy.

Another limitation of the 'Upper Body Model' is the used offset of the joint which connects the torso to the bicycle. L5 of the torso is connected 0.55 cm above the rear hub of the bicycle. Further analysis revealed that this offset was incorrect. In the experimental kinematic data from Dilgt [44], the vertical movement of the torso ranges between 0.87 m and 0.98 m (Figure 5.4.1).

The position and orientation of L5 of the spine, presented in Figure 5.4.1, are derived from the available dataset (Section 3.2.3). These positions are calculated in the local coordinate system of the bicycle frame.

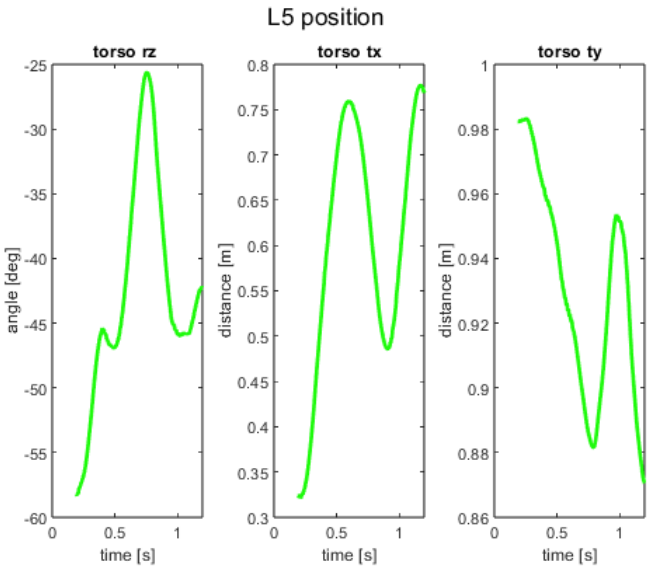

Figure 5.4.1: Position of the Torso at L5 in the Bicycle Frame Coordinate System. Torso at L5 horizontal translation, vertical translation and lean angle, from experimental data VU, calculated in the bicycle frame coordinate system.

While the 0.55 m offset model is not perfectly accurate, it still accounts for important factors such as the influence of the centre of mass location and its dependence on maximum crank torque. Therefore, it provides useful information on optimal movement and timing for BMX starts. However, exact joint angles should be interpreted with caution due to the simplified model and the incorrect offset.

To reduce computational time, the 'Upper Body Model' can still be utilized, but with a more accurate approximation of the inertia of the torso, and a planar joint between the torso and bicycle to better represent the real dynamics of BMX starts while maintaining computational efficiency.

Another limitation is the sensitivity to local minima in the predictive optimal control simulations. It was challenging to obtain a solution that deviated significantly from the initial guess with the 'Full Body Model'. The initial guess was the solution from the optimal tracking simulation. In the solution of the optimal tracking simulation, the bicycle pitch angle was large (this coordinate was not tracked since there was no IMU on the bicycle frame), and this was also seen in the predictive solution. The resulting angles were significantly higher than those measured in real life. In real life, balancing a bicycle with a high pitch angle is challenging. Perturbations require significant control and energy to maintain balance. In simulations, however, these perturbations are absent, and the optimization can perfectly determine the controls needed to counter any disturbances if they occur.

A cost term with a weight of 3 was used to minimize the frame pitch angle. Increasing the weight of this cost term further prevented the optimization from converging to an optimal solution using the 'Full Body Model'. Future work could include methods to better measure frame orientation, such as incorporating a new dataset that includes an IMU connected to the bicycle. This would allow for more

accurate tracking of the frame pitch angle, providing a better initial guess and potentially more realistic predictive simulation results.

The convergence tolerance of 10^{-3} used in the optimization process for the 'Full Body Model' may limit the precision of the results. This relatively loose tolerance was chosen to facilitate the optimization's convergence within a reasonable computational time. However, a tighter convergence tolerance could potentially yield more accurate and reliable solutions, although it would require significantly more computational resources. Future studies should explore the impact of different convergence tolerances further to ensure the robustness and accuracy of the optimization outcomes.

The damping in the joints during the BMX start simulations was higher than physiological levels due to the higher damping coefficients of 2.5 N·m/rad·s for the lower extremities compared to more accurate damping coefficients of around 0.1 N·m·s/rad in, for example, the knee [47]. This increased damping was necessary to ensure stability in the optimizations by reducing oscillations and preventing excessive joint movements, particularly with the 'Full Body Model'. Specifically, damping coefficients of 6.25 N·m·s/rad were used for the upper extremities and the torso coordinates, while the lower extremities had a damping coefficient of 2.5 N·m·s/rad.

The inverse kinematics should be redone using the same model as in the predictive or optimal tracking simulation to ensure consistency and accuracy in the joint angles and overall kinematics. Additionally, most changes to the model involved adjustments related to force dynamics. These changes do not influence the inverse kinematics. The only anthropometric change in the model was a different arm, which looked more realistic and was slightly longer, increasing by 3 mm between the shoulder and hand joint. However, the 'Full Body Model' was able to track these less accurate angles, suggesting that it would likely be capable of tracking more precise kinematics.

For the 'Full Body Model', a bidirectional coordinate coupler between crank rotation and rear wheel rotation was used. This coupling does not accurately reflect the true dynamics of the coupling between the cranks and rear wheel. However, we observed no negative net torque at the crank in the predictive study and only a brief occurrence of negative torque, approximately -50 Nm, in the optimal tracking simulation.

5.4.1. Future Research

One area for further research involves more extensive hypothesis testing using the 'Full Body Model'. Investigating various aspects of BMX start performance could provide deeper insights into optimizing this critical phase. For example, studying the differences in start performance with maximum strength differences between legs could reveal which leg should be the lead leg when there are asymmetries between the legs, or how technique changes with different rider strengths.

Another area of interest is the effect of different gear ratios on start performance, which could provide valuable information on how to optimize gear settings for maximum acceleration. Lastly, the impact of crank length on start performance could be explored to understand how different crank sizes affect leverage and force generation during the start. For these studies, it would be important to use a musculoskeletal model, since these parameters depend on specific muscle properties, like the force velocity and force length relationship. With a torque-driven model, you would not get reliable results.

These studies would provide a more comprehensive understanding of the biomechanics of BMX starts and could guide coaches and athletes in developing better training strategies and making informed equipment choices.

6

Conclusion

The primary goal of this research was to gain a deeper understanding of the mechanics of BMX gate starts using optimal control methods. By employing the OpenSim Moco platform and leveraging direct collocation techniques, we were able to optimize the complex biomechanics involved in BMX gate starts and identify key factors that influence performance.

Our study revealed several critical insights. First, the maximal crank torque significantly impacts the rider's kinematics, particularly influencing the recoil distance and the initial centre of mass location. Lower maximal crank torque resulted in a more backward position of the centre of mass and greater recoil, compared to higher maximal crank torque simulations.

The linear bicycle velocity between the initiation of the gate drop and the point where the gate is halfway open (0.52 s) was comparable for all simulation results, approximately matching the linear velocity of the gate. This finding suggests that the gate falling speed is the rate-limiting factor in the BMX start performance.

Additionally, a faster reaction time improves start performance; however, the start technique remained consistent across reaction times ranging from 0.14 s to 0.18 s.

The use of optimal control methods allowed us to simulate and analyse various scenarios, providing a systematic and analytic approach to studying BMX starts. These findings underscore the potential of optimal control techniques in enhancing athletic performance through detailed biomechanical analysis.

One limitation of this study is the simplified 'Upper Body Model,' which does not fully capture the complex biomechanics of a real BMX rider. Additionally, the use of a constant maximal crank torque does not reflect the true variability in torque during a real start. Future research could employ the 'Full Body Model' to gain deeper insights. This approach could address the limitations of the current study by incorporating more realistic biomechanical details and investigating other variables such as different rider strength, maximal force differences between legs, different gear ratios, and crank lengths.

In conclusion, this research provides valuable insights into the biomechanics of BMX gate starts and demonstrates the potential of optimal control methods in sports science. By advancing our understanding of these critical aspects, we pave the way for improved BMX start techniques and performance optimization in BMX racing. Future studies can build upon this framework to further explore and refine BMX start performance.

References

[1] J. C. Honea, "Beyond the Alternative vs. Mainstream Dichotomy: Olympic BMX and the Future of Action Sports," *Journal of Popular Culture*, vol. 46, no. 6, pp. 1253–1275, Dec. 2013, ISSN: 00223840. DOI: 10.1111/jpcu.12087.

[2] L. Rylands and S. J. Roberts, "Relationship between starting and finishing position in World Cup BMX racing," *International Journal of Performance Analysis in Sport*, vol. 14, pp. 14–23, 2014, ISSN: 14748185. DOI: 10.1080/24748668.2014.11868699.

[3] A. Daneshfar, C. Petersen, D. Gahreman, *et al.*, "Power Analysis of Field-Based Bicycle Motor Cross (BMX)," *Open Access Journal of Sports Medicine*, vol. Volume 11, pp. 113–121, Jul. 2020, ISSN: 1179-1543. DOI: 10.2147/OAJSM.S256052.

[4] U. C. Internationale. "BMX SX regulations." (2022), [Online]. Available: https://www.uci.org/regulations/3MyLDDrwJCJJ0BGGOFzOat#part-vibmx-racing (visited on 09/12/2022).

[5] M. A. D. Gross, F. Schellenberg, G. Lüthi, M. Baker, and S. Lorenzetti, "Performance determinants and leg kinematics in the BMX supercross start," *Journal of Science and Cycling*, vol. 6, no. 2, pp. 3–12, Dec. 2017, ISSN: 2254-7053. DOI: 10.28985/171231.jsc.08.

[6] J. D. C. Groenhuis, "A Good Beginning Makes a Good Ending," Ph.D. dissertation, Delft University of Technology, 2021.

[7] M. Kalichová, S. Hřebíčková, R. Labounková, P. Hedbávnỳ, and G. Bago, "Biomechanics analysis of bicross start," *International Journal of Sport and Health Sciences*, vol. 7, no. 10, pp. 614–622, 2013.

[8] M. Mateo, C. Blasco-Lafarga, and M. Zabala, "Pedaling power and speed production vs. technical factors and track difficulty in bicycle motocross cycling," *The Journal of Strength & Conditioning Research*, vol. 25, no. 12, pp. 3248–3256, 2011.

[9] M. Zabala, C. Sánchez-Muñoz, M. Mateo, *et al.*, "Effects of the administration of feedback on performance of the BMX cycling gate start," *Journal of Sports Science and Medicine*, vol. 8, no. 3, pp. 393–400, Sep. 2009, ISSN: 13032968.

[10] C. W. Herman, S. J. McGregor, H. Allen, and E. M. Bollt, "Power capabilities of elite Bicycle Motocross (BMX) racers during field testing in preparation for 2008 olympics.: 2321," *Medicine and Science in Sports and Exercise*, vol. 41, pp. 306–307, 2009.

[11] J. F. Cowell, M. R. McGuigan, and J. B. Cronin, "Movement and skill analysis of supercross bicycle motocross," *Journal of Strength and Conditioning Research*, vol. 26, no. 6, pp. 1688–1694, Jun. 2012, ISSN: 10648011. DOI: 10.1519/JSC.0b013e318234eb22.

[12] J. Grigg, E. Haakonsen, R. Orr, and J. Keogh, "Literature Review: Kinematics of the BMX SX Gate Start," *Journal Of Science & Cycling*, vol. 6, no. 1, Jun. 2017, ISSN: 22547053. DOI: 10.28985/171231.jsc.02.

[13] J. Grigg, "A biomechanical analysis of the bmx sx gate start," *Ph.D. dissertation, Bond University*, 2019.

[14] I. Janssen, A. Oude Alink, and F. Frielink, "Elite BMX Cyclist Use Individual Strategies For a Successful Start," *36th Conference of the International Society of Biomechanics in Sports*, pp. 126–129, 2018.

[15] P. Campillo, T. Doremus, and J.-m. Hespel, "Pedaling Analysis in BMX By Telemetric Collection of Mechanic Variables," *Brazilian Journal of Biomotricity*, vol. 1, no. 2, pp. 15–27, 2007, ISSN: 1981-6324.

[16] L. P. Rylands, S. J. Roberts, and H. T. Hurst, "Effect of gear ratio on peak power and time to peak power in BMX cyclists," *European Journal of Sport Science*, vol. 17, no. 2, pp. 127–131, Feb. 2017, ISSN: 15367290. DOI: 10.1080/17461391.2016.1210237.

[17] K. Gianikellis, A. Skiadopoulos, and A. Bote, “3d kinematics applied to the study of individual bmx gate start technique,” *Portuguese Journal of Sport Sciences*, vol. 11, 2 2011.

[18] A. Leggett. “Update: A post-mortem on the two-speed bmx bike that didn’t win the olympics.” (Aug. 2021), [Online]. Available: https://www.pinkbike.com/news/update-a-post-mortem-on-the-two-speed-bmx-bike-that-didnt-win-the-olympics.html (visited on 08/04/2023).

[19] L. P. Rylands, S. J. Roberts, H. T. Hurst, and I. Bentley, “Effect of cadence selection on peak power and time of power production in elite BMX riders: A laboratory based study,” *Journal of Sports Sciences*, vol. 35, no. 14, pp. 1372–1376, 2017, ISSN: 1466447X. DOI: 10.1080/02640414.2016.1215491.

[20] I. Janssen and J. Cornelissen, “Pedal forces during the BMX and track sprint cycling start,” *ISBS Proceedings Archive*, vol. 35, no. 1, p. 277, 2017.

[21] D. V. Knudson and D. Knudson, *Fundamentals of biomechanics*. Springer, 2007, vol. 183.

[22] M. L. Kaplan and J. H. Heegaard, “Predictive algorithms for neuromuscular control of human locomotion,” *Journal of Biomechanics*, vol. 34, no. 8, pp. 1077–1083, 2001.

[23] A. Zignoli, F. Biral, B. Pellegrini, A. Jinha, W. Herzog, and F. Schena, “An optimal control solution to the predictive dynamics of cycling,” *Sport Sciences for Health*, vol. 13, pp. 381–393, 2 2017, ISSN: 18247490. DOI: 10.1007/s11332-017-0370-9.

[24] D. B. Lipps, A. T. Galecki, and J. A. Ashton-Miller, “On the implications of a sex difference in the reaction times of sprinters at the beijing olympics,” *PLOS ONE*, vol. 6, e26141, 10 2011, ISSN: 1932-6203. DOI: 10.1371/JOURNAL.PONE.0026141. [Online]. Available: https://journals.plos.org/plosone/article?id=10.1371/journal.pone.0026141.

[25] T. Geijtenbeek, “Scone: Open source software for predictive simulation of biological motion,” *Journal of Open Source Software*, vol. 4, no. 38, p. 1421, 2019.

[26] C. L. Dembia, N. A. Bianco, A. Falisse, J. L. Hicks, and S. L. Delp, “Opensim moco: Musculoskeletal optimal control,” *PLOS Computational Biology*, vol. 16, no. 12, e1008493, 2020.

[27] M. Kelly, “An introduction to trajectory optimization: How to do your own direct collocation□,” *SIAM Review*, vol. 59, pp. 849–904, 4 2017, ISSN: 00361445. DOI: 10.1137/16M1062569.

[28] A. Wächter and L. T. Biegler, “On the implementation of an interior-point filter line-search algorithm for large-scale nonlinear programming,” *Mathematical programming*, vol. 106, pp. 25–57, 2006.

[29] S. L. Delp, F. C. Anderson, A. S. Arnold, *et al.*, “Opensim: Open-source software to create and analyze dynamic simulations of movement,” *IEEE transactions on biomedical engineering*, vol. 54, no. 11, pp. 1940–1950, 2007.

[30] A. Seth, J. L. Hicks, T. K. Uchida, *et al.*, “Opensim: Simulating musculoskeletal dynamics and neuromuscular control to study human and animal movement,” *PLoS computational biology*, vol. 14, no. 7, e1006223, 2018.

[31] S. L. Delp, J. P. Loan, M. G. Hoy, F. E. Zajac, E. L. Topp, and J. M. Rosen, “An interactive graphics-based model of the lower extremity to study orthopaedic surgical procedures,” *IEEE Transactions on Biomedical engineering*, vol. 37, no. 8, pp. 757–767, 1990.

[32] K. R. Holzbaur, W. M. Murray, and S. L. Delp, “A model of the upper extremity for simulating musculoskeletal surgery and analyzing neuromuscular control,” *Annals of biomedical engineering*, vol. 33, pp. 829–840, 2005.

[33] H. S. van Grieken, “Pedalling performance in the bmx supercross gate start,” *M.S. thesis, Delft University of Technology*, 2019.

[34] K. Kutzbach, “Mechanische leitungsverzweigung, ihre gesetze und anwendungen,” *Maschinenbau*, vol. 8, no. 21, pp. 710–716, 1929.

[35] A. Gordon, A. F. Huxley, and F. Julian, “The variation in isometric tension with sarcomere length in vertebrate muscle fibres,” *The Journal of physiology*, vol. 184, no. 1, pp. 170–192, 1966.

[36] A. V. Hill, “The heat of shortening and the dynamic constants of muscle,” *Proceedings of the Royal Society of London. Series B-Biological Sciences*, vol. 126, no. 843, pp. 136–195, 1938.

[37] M. Millard, M. Sreenivasa, and K. Mombaur, “Predicting the motions and forces of wearable robotic systems using optimal control,” *Frontiers in Robotics and AI*, vol. 4, pp. 1–12, Aug. 2017.

[38] W. McNally and J. McPhee, “Dynamic optimization of the golf swing using a six degree-of-freedom biomechanical model,” *Proceedings*, vol. 2, no. 6, p. 243, 2018.

[39] M. Yeadon and M. King, “Evaluation of a torque driven simulation model of tumbling,” *J. Appl. Biomech.*, vol. 18, pp. 195–206, 2002.

[40] D. Jones, J. Round, and A. De Haan, *Skeletal muscle: from molecules to movement*. Edinburgh, 2004.

[41] J. M. Winters and L. Stark, “Estimated mechanical properties of synergistic muscles involved in movements of a variety of human joints,” *Journal of biomechanics*, vol. 21, no. 12, pp. 1027–1041, 1988.

[42] Simbody, *Huntcrossleyforce class reference*, Online, Accessed: April 30, 2024. Available: `https://simtk.org/api_docs/molmodel/api_docs22/Simbody/html/classSimTK_1_1HuntCrossleyForce.html`, Mar. 2024.

[43] J. A. Andersson, J. Gillis, G. Horn, J. B. Rawlings, and M. Diehl, “Casadi: A software framework for nonlinear optimization and optimal control,” *Mathematical Programming Computation*, vol. 11, pp. 1–36, 2019.

[44] M. van Dilgt, “A new method to determine mechanical power output during the bmx gate start using inertial sensors,” *M.S. thesis, Vrije Universiteit Amsterdam*, 2020.

[45] N. Haralabidis, G. Serrancolí, S. Colyer, I. Bezodis, A. Salo, and D. Cazzola, “Three-dimensional data-tracking simulations of sprinting using a direct collocation optimal control approach,” *PeerJ*, vol. 9, Mar. 2021, ISSN: 2167-8359. DOI: `10.7717/PEERJ.10975`. [Online]. Available: `https://pubmed.ncbi.nlm.nih.gov/33732550/`.

[46] Y. C. Lin and M. G. Pandy, “Three-dimensional data-tracking dynamic optimization simulations of human locomotion generated by direct collocation,” *Journal of biomechanics*, vol. 59, pp. 1–8, Jul. 2017, ISSN: 1873-2380. DOI: `10.1016/J.JBIOMECH.2017.04.038`. [Online]. Available: `https://pubmed.ncbi.nlm.nih.gov/28583674/`.

[47] C. A. Oatis, “The use of a mechanical model to describe the stiffness and damping characteristics of the knee joint in healthy adults,” *Physical Therapy*, vol. 73, no. 11, pp. 740–749, 1993.

A

Figures

A.1. Simplified Upper Body Model

A.1.1. Initial Guess

The model for the optimal control problem during the separate recoil and forward phases was slightly different. The actuators used were coordinate actuators instead of activation coordinate actuators. In later optimizations, the model was incrementally made more complicated.

Figure A.1.1 displays the positions of all joints, except for the rear wheel and front wheel. Figure A.1.2 illustrates the joint torques and forces.

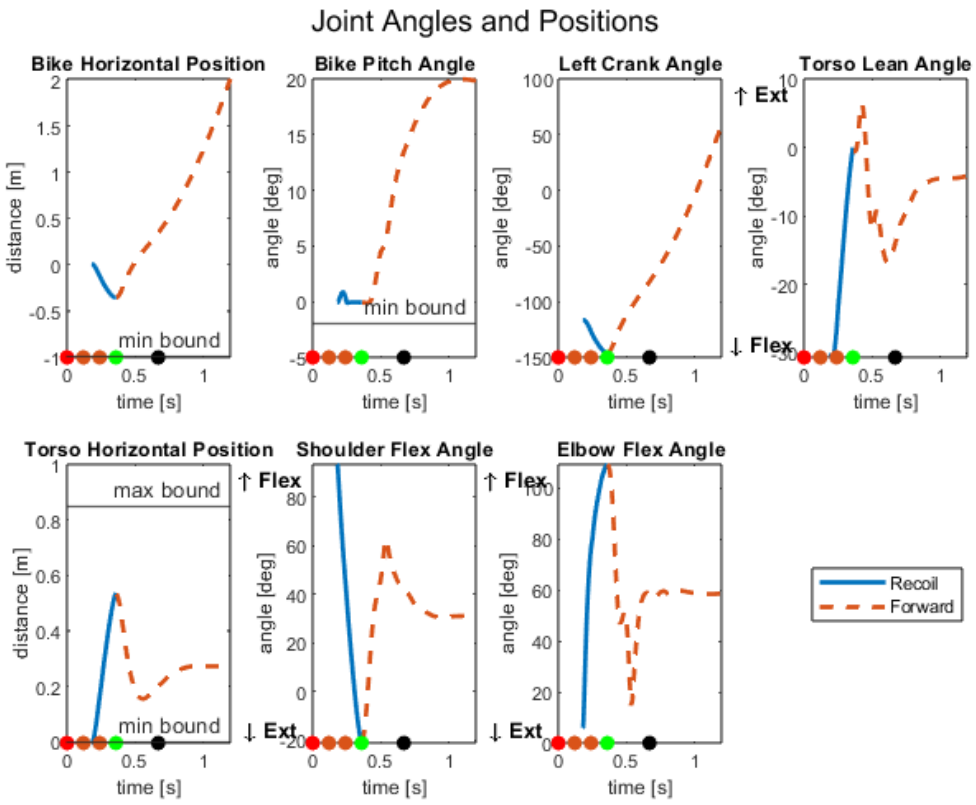

Figure A.1.1: Positions of All Joints for the Recoil and Forward Phases. The phases are simulated separately and used as the first initial guess (together with the joint velocities and control signals). The dots indicate the illumination of the start lights: red, first orange, second orange, and green. The gate starts opening at the green light and is fully open at the final black dot.

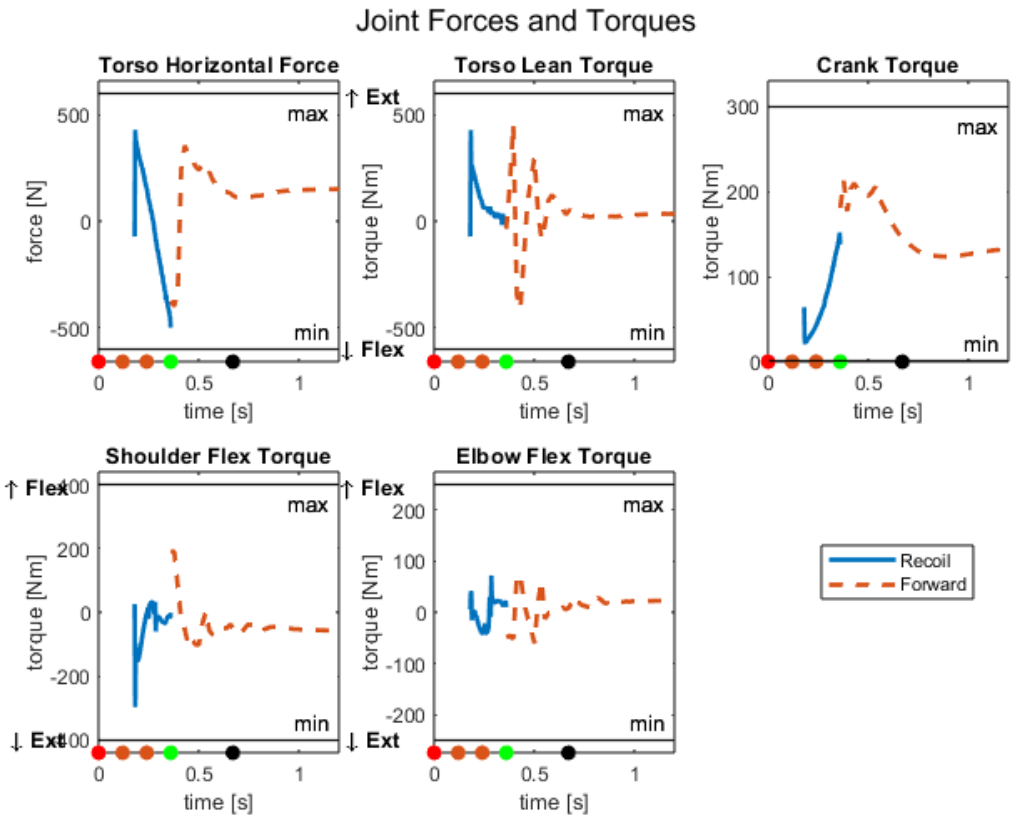

Figure A.1.2: Forces and Torques Of Joints for Recoil and Forward Phases. The phases are simulated separately and used as the first initial guess (together with the joint velocities and positions). The dots indicate the illumination of the start lights: red, first orange, second orange, and green. The gate starts opening at the green light and is fully open at the final black dot.

A.1.2. Different maximal Crank Torques

	Initial Position					
	250 Nm	**275 Nm**	**300 Nm**	**325 Nm**	**350 Nm**	**Experimental VU**
Crank Angle l	81.17°	81.17°	81.17°	81.17°	81.17°	81.17°
Torso Lean	-45.00°	-35.96°	-25.48°	-16.68°	-14.85°	-58.23°
Torso Translation	0.06 m	0.12 m	0.20 m	0.25 m	0.26 m	0.32 m
Shoulder Flexion	103.66°	90.46°	76.14°	73.92°	73.92°	69.95°
Elbow Flexion	26.11°	26.11°	26.11°	9.87°	5.71°	20.69°
	Final Position					
Bike Translation	3.59 m	3.82 m	4.08 m	4.30 m	4.50 m	2.96 m*
Bike Pitch	1.03°	1.04°	1.04°	1.05°	1.05°	N/A
Crank Angle l	382.86°	402.42°	423.96°	443.34°	460.10°	326.87°
Torso Lean	-5.98°	4.43°	7.43°	9.08°	10.53°	-42.33°**
Torso Translation	0.42 m	0.50 m	0.55 m	0.60 m	0.63m	0.77 m*
Shoulder Flexion	30.24°	17.56°	9.16°	-0.62°	-6.19°	-3.81°
Elbow Flexion	62.04°	65.30°	73.00°	83.34°	88.35°	56.19°

Table A.1.1: Initial and Final Positions for Different Maximal Crank Torque Values. The initial and final positions are shown for crank torques of 250Nm, 275Nm, 300Nm, 325Nm, and 350Nm, as well as the experimental value from the VU. *calculated from rear wheel rotation, **calculated from the position of lumbar vertebra 5 (L5) at the torso in the local coordinate system of the bicycle.

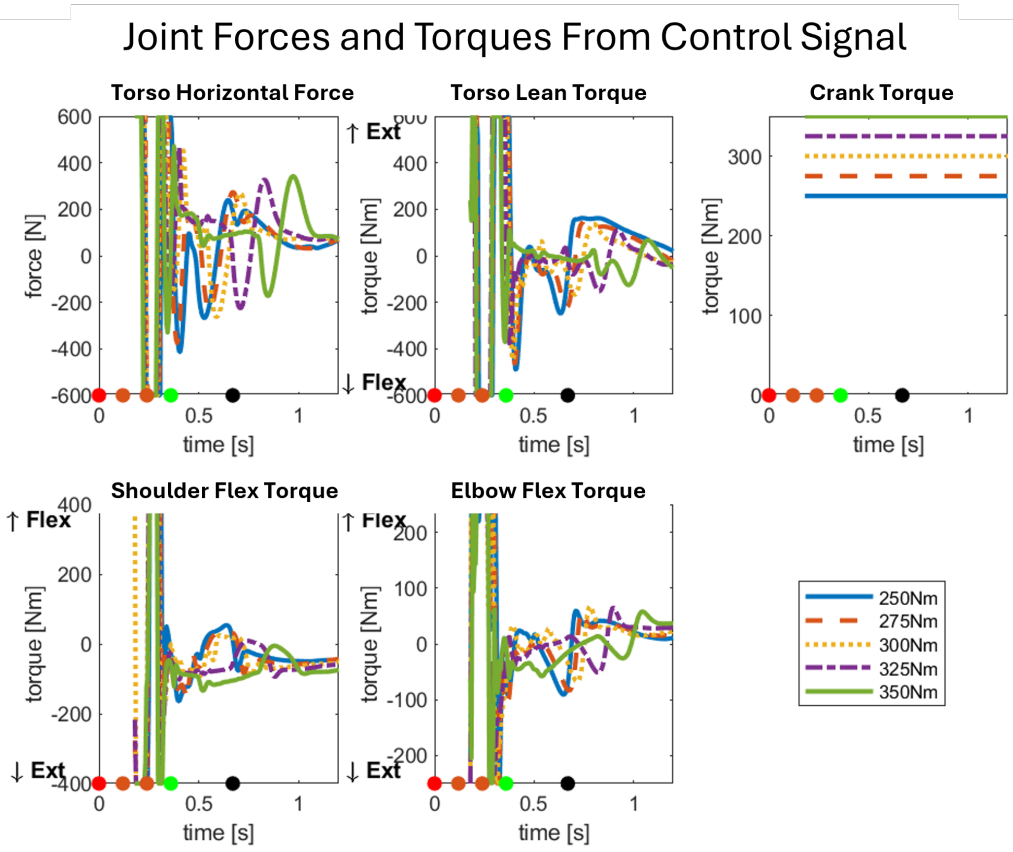

Figure A.1.3: Joint Forces and Torques From Controls Signal for Different Maximal Crank Torques. The lower and higher y limits of the y-axis are the minimal and maximal joint force or torque (except for the bracket torque). This figure illustrates the control inputs for various maximal crank torques.

A.1.3. Different Reaction Times

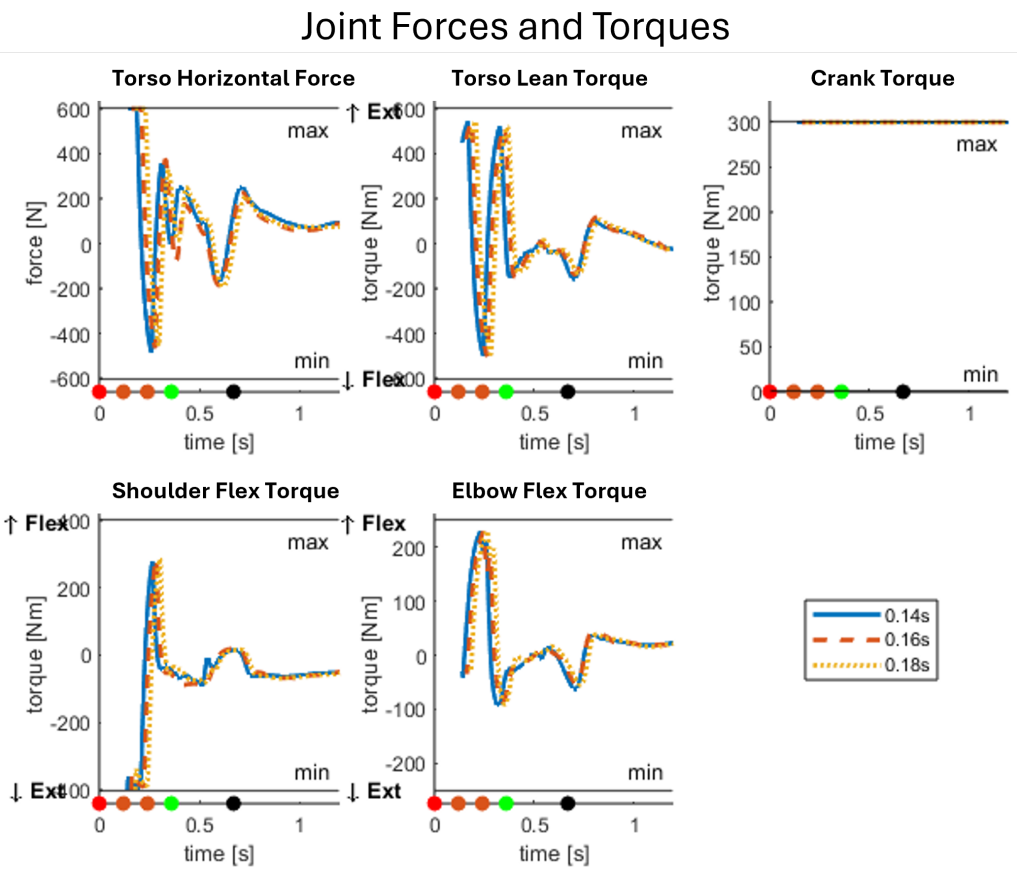

Figure A.1.4: Joint Forces and Torques for Different Reaction Times. This graph details the Forces and Torques at various joints for three reaction times (0.14 s, 0.16 s and 0.18 s). The horizontal lines depict the minimal and maximal force/torque of the actuator. The dots indicate the illumination of the start lights: red, first orange, second orange, and green. The gate starts opening at the green light and is fully open at the final black dot.

B

Moco Study

In this Appendix, the Moco setup file is displayed. The OpenSim model has been stripped out, and is replaced with the line '<!– The OpenSim model is typically included here –>'. Access to the model is restricted to approved individuals to prevent competitive exploitation. Additionally, explanatory comment lines, written between '<!– .–>', have been omitted to streamline the document.

```
<?xml version="1.0" encoding="UTF-8" ?>
<OpenSimDocument Version="40000">
  <MocoStudy name="OneMotion_300Nm">
    <write_solution>true</write_solution>
    <MocoProblem name="problem">
      <MocoPhase name="phases">
        <ModelProcessor name="model">
          <model>
            <Model name="UpperBody_Model">
              <!-- The OpenSim model is typically included here -->
            </Model>
          </model>
        </ModelProcessor>
        <MocoInitialBounds name="time_initial_bounds">
          <bounds>0.17999999999999999</bounds>
        </MocoInitialBounds>
        <MocoFinalBounds name="time_final_bounds">
          <bounds>1.5</bounds>
        </MocoFinalBounds>
        <state_infos>
          <MocoVariableInfo name="/jointset/rearWheelToFrame/rearWheel_angle/value">
            <bounds>-15 75</bounds>
            <initial_bounds></initial_bounds>
            <final_bounds></final_bounds>
          </MocoVariableInfo>
          <MocoVariableInfo name="/jointset/frontWheelToFrame/frontWheel_angle/value">
            <bounds>-15 75</bounds>
            <initial_bounds></initial_bounds>
            <final_bounds></final_bounds>
          </MocoVariableInfo>
          <MocoVariableInfo name="/jointset/bracketToFrame/crank_angle_l/value">
            <bounds>-5 25</bounds>
            <initial_bounds>1.4166475731684041</initial_bounds>
            <final_bounds></final_bounds>
          </MocoVariableInfo>
          <MocoVariableInfo name="/jointset/frameToPlatform_tx/frame_tx/value">
            <bounds>-2 15</bounds>
            <initial_bounds>0</initial_bounds>
            <final_bounds></final_bounds>
          </MocoVariableInfo>
          <MocoVariableInfo name="/jointset/frameToPlatform_rz/frame_rz/value">
            <bounds>-0.017453292519943295 0.52359877559829882</bounds>
            <initial_bounds>7.3803973458684684e-14</initial_bounds>
            <final_bounds>-0.01745 0.01745</final_bounds>
```

```
    </MocoVariableInfo>
    <MocoVariableInfo name="/jointset/shoulder_r/shoulder_angle_r/value">
      <bounds>-1.5707963705062866 3.1415927410125732</bounds>
      <initial_bounds>1.2902221439658799 1.9883538447636118</initial_bounds>
      <final_bounds>0 1</final_bounds>
    </MocoVariableInfo>
    <MocoVariableInfo name="/jointset/elbow_r/elbow_angle_r/value">
      <bounds>0 2.268928050994873</bounds>
      <initial_bounds>0 0.45565254959067403</initial_bounds>
      <final_bounds>1.1 1.5</final_bounds>
    </MocoVariableInfo>
    <MocoVariableInfo name="/jointset/torso_rz_and_tx/torso_rz/value">
      <bounds>-0.78539999999999999 0.78539999999999999</bounds>
      <initial_bounds>-0.78539999999999999 -0.18743632375376601</initial_bounds>
      <final_bounds></final_bounds>
    </MocoVariableInfo>
    <MocoVariableInfo name="/jointset/torso_rz_and_tx/torso_tx/value">
      <bounds>0 0.84999997615814209</bounds>
      <initial_bounds>0 0.35306710682081085</initial_bounds>
      <final_bounds></final_bounds>
    </MocoVariableInfo>
    <MocoVariableInfo name="/jointset/gateToPlatform/gate_rz/value">
      <bounds>0 1.570796326794897</bounds>
      <initial_bounds>1.2217304763960311 1.570796326794897</initial_bounds>
      <final_bounds></final_bounds>
    </MocoVariableInfo>
    <MocoVariableInfo name="/jointset/frameToPlatform_tx/frame_tx/speed">
      <bounds>-20 20</bounds>
      <initial_bounds>0</initial_bounds>
      <final_bounds></final_bounds>
    </MocoVariableInfo>
  </state_infos>
  <state_infos_pattern>
    <MocoVariableInfo name="/jointset/.*/speed">
      <bounds>-100 100</bounds>
      <initial_bounds>0</initial_bounds>
      <final_bounds></final_bounds>
    </MocoVariableInfo>
  </state_infos_pattern>
  <control_infos>
    <MocoVariableInfo name="/forceset/torso_tx_Force">
      <bounds>-1 1</bounds>
      <initial_bounds></initial_bounds>
      <final_bounds></final_bounds>
    </MocoVariableInfo>
    <MocoVariableInfo name="/forceset/torso_rz_Torque">
      <bounds>-1 1</bounds>
      <initial_bounds></initial_bounds>
      <final_bounds></final_bounds>
    </MocoVariableInfo>
    <MocoVariableInfo name="/forceset/bracket_Torque">
      <bounds>0 1</bounds>
      <initial_bounds></initial_bounds>
      <final_bounds></final_bounds>
    </MocoVariableInfo>
    <MocoVariableInfo name="/forceset/shoulder_rz_Torque">
      <bounds>-1 1</bounds>
      <initial_bounds></initial_bounds>
      <final_bounds></final_bounds>
    </MocoVariableInfo>
    <MocoVariableInfo name="/forceset/elbow_rz_Torque">
      <bounds>-1 1</bounds>
      <initial_bounds></initial_bounds>
      <final_bounds></final_bounds>
    </MocoVariableInfo>
  </control_infos>
  <goals>
    <MocoControlGoal name="myeffort">
      <weight>0.01</weight>
      <divide_by_displacement>true</divide_by_displacement>
    </MocoControlGoal>
```

```
        <MocoOutputGoal name="outputGoalBikeVelocity">
          <weight>-0.80000000000000004</weight>
          <output_path>/bodyset/frame|linear_velocity</output_path>
          <exponent>1</exponent>
          <output_index>-1</output_index>
          <divide_by_displacement>false</divide_by_displacement>
        </MocoOutputGoal>
        <MocoFinalOutputGoal name="finalOutputGoalPosition">
          <weight>-0.20000000000000001</weight>
          <output_path>/bodyset/frame/frame_offset_Fronthub|position</output_path>
          <output_index>-1</output_index>
        </MocoFinalOutputGoal>
        <MocoStateTrackingGoal name="minimizeFrame_rz">
          <weight>3</weight>
          <mode>cost</mode>
          <TableProcessor name="reference">
            <filepath>frame_rz_zero.sto</filepath>
            <operators>
              <TabOpLowPassFilter>
                <cutoff_frequency>-1</cutoff_frequency>
              </TabOpLowPassFilter>
            </operators>
          </TableProcessor>
          <allow_unused_references>false</allow_unused_references>
        </MocoStateTrackingGoal>
      </goals>
    </MocoPhase>
  </MocoProblem>
  <MocoCasADiSolver name="solver">
    <num_mesh_intervals>250</num_mesh_intervals>
    <transcription_scheme>hermite-simpson</transcription_scheme>
    <optim_max_iterations>10000</optim_max_iterations>
    <optim_convergence_tolerance>0.00001</optim_convergence_tolerance>
    <optim_constraint_tolerance>0.001</optim_constraint_tolerance>
    <guess_file>OneMotion_300Nm_frontwheelContact_2_diff_torsoOff_solution.sto</guess_file>
    <optim_finite_difference_scheme>forward</optim_finite_difference_scheme>
  </MocoCasADiSolver>
 </MocoStudy>
</OpenSimDocument>
```